MAGNETITE DOPED CARBON AS A SUBSTRATUM FOR NERVE CELL CULTURE

Major Qualifying Project Report completed in partial fulfillment of the Bachelor of Science degree in Chemical Engineering at Worcester Polytechnic Institute, Worcester, MA

Submitted to:

Professor Hong Suzan Zhou (advisor)

Oljora Rezhdo

_____

Matthew Perrone

_____

4/29/2010

Acknowledgements

We would like to thank Professor Susan Zhou for her continued support throughout the project as well as the students in her lab, Dr. Jiaolong Wang, Post-Doctorate research fellow and Zanzan Zhu, Ph.D. candidate. Another special thank you goes to professor Zheng-Zheng Bao at the University of Massachusetts Medical School and her students, Dr. Dong Han and Post-Doctorate research fellow and Daorong Guo, Ph.D. candidate. We are also thankful to Sena Ada, M.S. candidate in Professor Terri Camesano's lab for her help with the AFM machine, Ann Plona, Ph.D. candidate in Professor W. Grant McGimpsey's lab for her help with the goniometer, and Professor Peter Hefti, in the Mechanical Engineering Department for his support with our experiments in the clean room, as well as Rick Pampuro, current Ph.D candidate at Cornell who pioneered much of the work on this project as his undergraduate MQP. This project would not have been possible without their patience and support.

Abstract

A biocompatible, photoresist derived, thin carbon substrate has been recently developed which promotes nerve proliferation and differentiation. A method which alters the substrate's physical and electrochemical properties by doping photoresist with magnetite nanoparticles has been developed to enhance the existing substrate's ability to foster cell growth. Rat pheochromocytoma cells were used for culture to test substrate-cell interactions. Varying the nanoparticle concentration on the surface produced increased surface roughness, electrical conductivity, cell concentration and average neurite length.

Table of Contents

Table of Figures

1 Introduction

Brain and spinal cord injuries have some of the most fatal consequences to humans. They are directly related to the nervous system which has been previously shown to have limited abilities to heal and regenerate, even though the causes and mechanisms are poorly understood. However, neuroregenerative medicine, despite the many technical and practical challenges, is of particular importance in treatment strategies of such disorders that would prove beneficiary to patients. Nerve cells, being the main unit of the nervous system, require a detailed study of the cellular genetic and signaling pathway to be able to find the techniques to cure most neural diseases.

However, cells are not directly accessible in vivo and therefore their properties cannot be measured by methods that require direct contact between probe and cell. A fairly recent technology called microelectromechanical systems (MEMS) has been used to design a substratum available to cellular adhesion, growth and development, giving the researchers the opportunity to artificially, in-vitro, create the specific microenvironment found within the body. MEMS have been especially developed in the last twenty years, serving initially different purposes such as in the fields of microfluidics, aerospace, wireless communications, data storage, optics, etc. More recently they have attracted biomedical and chemical scientific interest in the production of biosensors such as DNA detection[1], blood glucose levels determination[2], narcotic abuse testing applications[3], etc.

More specifically, our MEMS fabrication technique utilizes silicon wafers coated with a photoresistive material doped with nanoparticles. The technique replicates the photolithographic procedure followed by pyrolysis to create a carbon layer compatible for neuronal growth. The material can also be easily patterned depending on the experiment's goals. This fabrication procedure is advantageous in the substrates capacity to be easily modified in terms of mechanical properties such as roughness, hardness, electrical conductivity, surface energy etc. simply by altering the type of nanoparticles and their concentration. Furthermore, being cost efficient, the material would also be commercially attractive.

This project refines the broad application of MEMS with the nervous system to improve the material's physical properties in a way that is most advantageous to cell growth and differentiation. Our material was tested for surface energy, roughness, and electrical conductivity. Magnetite was used as the base nanoparticle. Three different nanoparticle concentrations were tested for the properties just mentioned as well as in cellular assays. PC-12 cells, which were used for our experiments, represent a cell line that comes from the rat's adrenal gland. The most optimal substrate that promotes cell proliferation and differentiation was therefore determined.

[1] (Schreier, 2005)
[2] (Xian Huang, 2009)
[3] (Pohanka, Jun, & Kuca, 2007)

2 Background

2.1 The Nervous System

The nervous system is one of the four body systems, that controls all metabolic processes by chemically and electrically transmitting signals, impulses from the brain to the different organs of the body. It is divided into the Central Nervous System (CNS) and the Peripheral Nervous System (PNS). The CNS consists of the brain and the spinal cord, while the PNS includes all the nerve extensions ending in all organs forming a web that spreads throughout the entire organism.

2.1.1 The Central Nervous System

The brain is the most complex organ in the human body. Although it works as a unified whole, neuroscientists have identified three interconnected layers that perform specific functions: the central core, the limbic system, and the cerebral cortex, which regulate the everyday life activities.

The central core consists of five main regions that regulate processes such as breathing, pulse, arousal, movement, balance, sleep, and the early stage of processing sensory information. These regions include the thalamus, the pons, the cerebellum, the reticular formation, and the medulla. The thalamus interprets sensory information such as touch, hearing, vision etc, and then forwards the information to the appropriate region in the cerebral cortex where the information processing continues. The pons triggers dreaming and waking from sleep. The cerebellum coordinates the body movement, posture, and equilibrium. The reticular formation sends signals to the cerebral cortex to remain alert even during sleep. The medulla is the center for breathing, waking, sleeping, and heart beating.[4]

The limbic system consists of three regions that mediate behaviors, emotional states, and memory processes. Furthermore, it regulates the body temperature, blood pressure, blood sugar levels etc. These three regions are the hippocampus which is important in emotions, learning, and memory, the amygdala which plays a role in aggression, eating, drinking, and sexual behaviors, and last the hypothalamus which monitors glucose blood levels, salt, blood pressure, and hormones.[4]

The cerebral cortex directs the brain's higher cognitive and emotional functions. It is divided into two symmetrical hemispheres containing each four lobes, the frontal, occipital, parietal, and temporal lobes. These areas oversee all conscious experiences including perception, emotion, thought, and planning, as well as many unconscious cognitive and emotional processes.[4]

All these brain functions have been studied and determined through electroencephalography (EEG) which records the electrical activity based on which part of the brain fires signals. Although so much is known, groundbreaking research is being done to fully understand the effects of sleep in the organism, the causes of memory-impairing conditions such as Alzheimer's, the understanding of the processing of visual information and how it is transferred to different lobes in an effort to cure dyslexia etc.

The spinal cord consists of nervous tissue whose function consists only in the transmission of neural signals between the brain and the rest of the body. Another small but very important task of the spinal

[4] (Foundation, 2001)

cord is that of the neural circuits that control reflexes and central pattern generators.[5] The inner region consists of grey matter which includes neural cell bodies, glia, and capillaries. In living tissue this color is grey-pinkish because of the capillary blood vessels and of the cell bodies. The peripheral region is surrounded by white matter composed of bundles of nerve cell extensions that connect the grey matter to the PNS as well as to the cell bodies in the grey matter itself by transmitting nerve impulses.

2.1.2 The Peripheral Nervous System

The PNS consists of two types of cells, the sensory (afferent) nerves that carry information from the organs or external stimuli to the CNS, and the motor (efferent) nerves that transmit messages from the CNS to the organs and limbs. The motor nervous system in itself is divided into the somatic and the autonomic nervous system. The somatic nervous system enables voluntary movement of skeletal muscles all over the body. It also reports their current state or position in order for us to know our capabilities at any given time. Reflexes are an exception. The internal organs are controlled by the autonomic nervous system. Some parts of this system can be consciously overridden such as conscious quick breathing; however, most parts cannot be controlled. It sends information to three types of tissues, the cardiac muscle found in the walls of the heart, the smooth muscle found in the blood vessels, bladder, uterus, gastrointestinal tract, respiratory tract, ciliary muscle and iris in the eye, and arrector pili of skin, or glandular tissue which synthesizes hormones. The autonomic nervous system is made of the sympathetic and the parasympathetic nervous systems. The sympathetic nervous system arouses internal organs when the body faces challenging external stimuli. In such a case it dilates the pupils, accelerates heartbeat, inhibits digestion, stimulates glucose release from the liver, stimulates the adrenal glands to release adrenaline and noradrenaline, and finally it relaxes the bladder. The parasympathetic nervous system generates the opposite effect. This happens in the situation where there are no external challenges, which we most frequently encounter. In such a case it contracts the pupils, decreases the heartbeat, stimulates digestion and the gallbladder, and contracts the bladder. Both systems work together to maintain homeostasis.

2.1.3 The Neuron

The smallest microscopic unit of the nervous system is the neuron. A neuron is a cell specialized in transmitting impulses, electrical and/or chemical, from the brain and spinal cord to the rest of the body and vice-versa. The neuron's structure consists of the dendrites, the cell body (soma), the axon and the axon terminal. The dendrites receive the signal and convert it to electrical by creating a potential difference between the inside and the outside. Such a potential difference is generated by the different ionic charges and concentrations of K^+, Na^+, and Cl^-. One neuron can have up to 2000 dendrites, allowing it to better receive and transmit information.[6] The soma represents the main body of the cell with all the different organelles including the nucleus. It collects the stimulus coming from the dendrites as shown in Figure 1, and then it fires through the axon, the longest extension of the cell wall. In the axon terminal there are the synaptic end bulbs where the electrical signal causes the neurotransmitters, small vesicles found in the tip of the axon, to release a chemical called acetylcholine into the synaptic gap between the neuron and the other tissue which usually ends in another neuron or less frequently a muscle.

[5] (Jean Hopkins, 2003)
[6] (Boston, 2007)

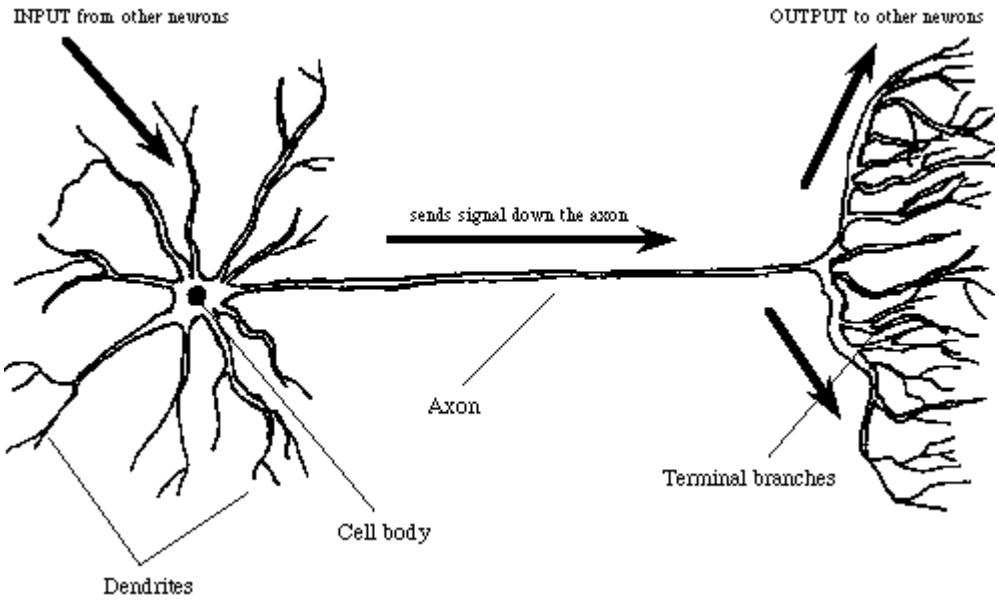

Figure 1: Structure of the neuron[7]

Structurally, based on the number of dendrites extending from the cell body, neurons can be divided into unipolar, bipolar, and multipolar. A unipolar neuron contains one axon and no dendrites; a bipolar neuron contains one axon and one dendrite, and a multipolar that has one axon and multiple dendrites. For obvious reasons the majority of neurons in the CNS are multipolar.

Based on their function neurons can be divided into three main groups, afferent, efferent and interneurons. The afferent neurons form the sensory nervous system, i.e. they carry information from the limb receptors and organs to the CNS. Structurally they differ in the fact that the dendrites are long and the axon is short contrary to efferent neurons. However, the signal flow is always from the dendrite to the cell body to the axon and finally to the axon terminal. These neurons form synapses with other afferent neurons as well as with interneurons, which are found in the CNS, and more specifically in the spinal cord. Interneurons serve as connectors between the afferent and the efferent neurons. In shape they are very similar to efferent but they differ in cell size. Interneurons are very small, with a much shorter axon, although relatively longer than the dendrites. In function they use a different kind of neurotransmitter which releases glycine or glutamate, as opposed to acetylcholine. Interneurons are always found in the CNS. Efferent neurons also known as motor or effector neurons transmit the signal from the CNS to the organs. Their soma is found in the CNS while their axons project into most organs. Efferent neurons form synapses only with muscles.

2.1.4 Nerve Regeneration Dichotomy

For several decades it was believed that neurogenesis, the regeneration of neurons, is impossible and that we are born with a finite amount of grey matter in our body. However, deeper studies have been performed over the years and such a statement has proved to not be completely correct. It is true that these neurons cannot perform mitosis, i.e. cell division; however, there is a layer of stem cells in the

[7] (Nerve Regeneration)

hippocampus which produces a steady stream of neurons which with the help of the cerebrospinal fluid can migrate outwards to the cerebral cortex. This fact was initially noticed in adult monkeys in 1999[8],[9], and later in 2003 in humans[10]. This is considered as the first scientific proof of the ability of the CNS to regenerate. On the other hand, because of their long structure axons are the most easily damaged part of the neuron. To date there is no convincing scientific explanation for the inability of the CNS axons to re-innervate although several tests have been performed. The neurons that form the PNS, on the other hand, allow regeneration because of a structural difference compared to the CNS neurons. These axons on top of the myelin sheath contain Schwann cells, which are rich in extracellular matrix constituents such as laminin, collagen, fibronectin, entactin, and heparin sulphate. [11] Later evidence showed that Schwann cells deprived of axonal contact produce nerve growth factor (NGF), a protein with neuro-regenerative capabilities, encouraging therefore peripheral nerve regeneration. [12] An interesting experiment was performed by several groups of researchers over the course of the years, starting from 1911, during which severed CNS neurons were placed in an environment in which PNS axons are able to regenerate. More specifically, segments of peripheral nerve were grafted into the CNS, and it was demonstrated that CNS axons are capable of extending considerable distances within the environment of a peripheral nerve, although when re-directed back into the CNS further axon elongation is arrested.[13] These experiments have given substantial evidence that, when provided with an appropriate environment, central axons will regenerate over significant distances and are able to form synaptic contact with target cells.[13]

2.2 PC-12 Cell Culture

For this project one type of cell was used, PC-12 cells, which consititute a cell line as opposed to what we are used of thinking as regular CNS or PNS primary neurons. A cell line differs from a cell strain in the fact that these cells have escaped the Hayflick limit, the point at which the cell is not any more capable of dividing due to the shortening of telomeres inside the cell at each division step. The cell line is usually an abnormal, mutated cell strain that is immortalized, i.e. that can divide infinitely as long as the appropriate growth media is supplied. On the other hand a primary neuron is the first in the motor pathway is then followed by secondary and tertiary neurons consecutively.

PC-12 cells were first discovered in the mid-1970s by Greene and Tischler.[14] They are a cell line established from rat adrenal pheochromocytoma. PC-12 cells have been shown to respond effectively to Nerve Growth Factor (NGF) by ceasing their proliferation process and by causing neuronal differentiation through the long extensions of the membrane. Clonal cell lines which express neuronal properties are useful models for studying the nervous system at the molecular level.[14] After their discovery, several tests were performed on this particular molecule. However, the major focus has been on understanding the signaling pathway during PC-12 differentiation. Understanding such a process is

[8] (Howard, 1999)
[9] (Olle Lindvall, 2003)
[10] (Ming Zhao, 2003)
[11] (Bunge, 1983)
[12] (Johnson, 1988)
[13] (R.J.M. Franklin, 1990)
[14] (Lloyd A. Greene, 1976)

advantageous since the induction of a certain element of the pathway can promote different outcomes such as neuritogenesis, gene induction, and proliferation.[15] In the long run, such a process would allow flexibility in experimenting with human nerve cells, by adopting the same pathway.

2.3 Substrate Fabrication

The choice of our substrate was based on several factors. Many different materials have been considered for use in tissue engineering in the past decade, including carbon, glasses, polymers, and composite materials. For our study, we required a substrate that can be made in-house, can be made repeatedly, be biocompatible, and have tunable electromechanical properties.

The use of carbon nanotubes as substrates for neuronal cell growth has been experimented with in the past decade, with focus put on the fabrication of the nanotubes and the various modifications that could be made to them. Once such study tested chemically functional nanotubes, investigating the cell morphology between different groups, as different groups will confer different properties to the surface of the carbon. The University of California team was able to manipulate the charge carried by the functional groups and could crudely control the outgrowth and branching pattern of the neurons that were cultured.[16] A patent was filled in 2003 for ways to test the nanostructures as promoters of neuronal cell growth, with hope to lead to bimolecular implants for nerve regeneration.[17]

While other materials can be used, we believe that carbon-based substrates have the most potential when it comes to modification, with parameters of hardness, roughness, thickness, surface energy, and electrical resistivity that can be modified and tuned with the fabrication process. Polymers, such as polyethylene-glycol (PEG) and polymethylmethacrylate (PMMA), while being easy to work with (translucent, injection moldable, cheap), have little ability to be modified with anything but different coatings. Polyurethanes, such as the non-toxic, biodegradable LDI-based urethanes studied by a University of Pittsburg group, have proven biocompatibility, but may only be able to find a niche in terms of tissue engineering, as thought the urethane is stable and can be sterilized, the properties are fairly fixed in terms of hardness, with little electrical potential as a it is a fairly good insulator.[18]

The complexity of other material fabrication, such as zeolytes, the already-proven potential for carbon, and the many tunable parameters of a thin carbon film make a carbon surface the main focus of our research.

2.4 Epoxies and Photolithography

In order to fabricate a thin film, there needs to be the source of the carbon. While many options exist, an epoxy precursor was chosen as it is already used in the field of micro-electromechanical systems (MEMS) and can undergo pyrolysis, burning is an inert environment, to reduce the epoxy down to a 99.5% pure carbon surface.

[15] (D. Vaudry, 2002)
[16] (Hui Hu, 2004)
[17] (Mattson, Dec 30, 2003)
[18] (Jian Ying Zhanga, June 2000)

Epoxies have a wide range of applications; the uses of epoxy monomers are seen in composite materials. In the realm of structural composites, epoxy monomers are used as a base for thermoset resin systems that are coupled with a structural fiber. In the case of aerospace, this technical fiber is commonly carbon fiber. The high cost of the coating, layup, and curing process, as well as the difficulty in automating the process has driven a search for alternative methods of creating epoxy-matrix composites. One method found of polymerizing an epoxy-fiber matrix is through cationic polymerization, achieved by bombarding the epoxy with a beam of electrons; locally, this will cure the sample at room temperature, as opposed to at elevated temperature and pressure over time. This alternative method requires, however, oxygen and water free environments, and, at the time of study, a large amount of energy to successfully polymerize the epoxy.[19]

In the realm of epoxies, a subset exists under the name of "photoresitive epoxy". These epoxies are UV active, and can be "etched" on a micron scale. The epoxy is coated, via spin coating, onto a wafer substrate. These wafers can be made of silicon, glass, quartz, crystalline Ge, SiC, GaAs, GaP or InP. Once the photoresist is coated on the wafer, a small part or complex set of parts can be fabricated through various methods; the most common are UV photolithography, iso/aniso-tropic wet etching and dry etching. Wet etching typically uses either a strong alkaline base such as TMAH or KOH (anisotropic), or acids such as HF or H2SO4 (isotropic), whereas dry etching uses a gaseous substance to remove the epoxy through a chemical reaction. [20]

Epoxy-based MEMS have been used extensively in research with human cells. One example is, in 2008, a study was undertaken to test the elasticity of human oocytes. By fabricating two very thin epoxy beams, the cell could be fit between two orthogonal beams and pressed, with imaging equipment used to determine the displacement, and therefore the elasticity. The small epoxy parts were etched from a silicon wafer spin-coated with SU-8.[21] Please consult section 2.5.1 for further C-MEMS applications.

2.4.1 Pyrolysis

Pyrolysis is a procedure of heating a sample to high temperatures in an inert environment. This process is used in many facets of organic materials workmanship, be it forming syngas from biomass fuels to the production of carbon fiber filaments. By heating a precursor material in such an environment, the substance does not react, therefore off-gassing hydrocarbons (typically methane, CH_4) and leaving a carbon residue behind; this process is also known as carbonization. Epoxies, as detailed before, are a hydrocarbon that, when pyrolyzed, will leave a thin carbon residue.

Pyrolysis of patterned photoresist was first undertaken in the semiconductor industry to create carbon microstructures as well as thin carbon films. A group at AT&T Laboratories in New Jersey was looking for an alternative way to fabricate microstructures; the common method was etching, which was time consuming and chemically hazardous. By patterning the photoreactive epoxy HPR-206 with UV and then pyrolyzing, the team found that "the preparation of patterned films from pyrolyzed photoresist eliminates several processing steps and demonstrates the potential of direct lithography of carbon for

[19] (James V. Crivello, 1997)
[20] (Chollet, 2009)
[21] (Bruno Wacogne, 2008)

integrated circuit manufacture"; with this alternative becoming not only suitable but favored, much attention was then focused on the production of microstructures derived from this procedure.[22,23]

The ability to modify the properties of the microstructures through the pyrolysis procedure (maximum temperature, ramp temperature, etc) is a function of the crosslinking that is occurring in the epoxy. A polymer, epoxies will undergo a crosslinking reaction, with C-O bonds (found in the C-O-H form) turning into C=O bonds (in the form of C-O-C). This can be seen through X-ray photoelectron spectroscopy (XPS); there is a clear shift between C-O and C=O bonds with an increase in pyrolysis temperature. This crosslinking greatly increases the hardness and rigidity of the epoxy structure, as well as off-gasses hydrogen and carbon that are freed due to the increase in energy (C-C, O-H bonds break, typically off-gassing H_2 and CH_4). This also lowers the ratio of oxygen to carbon in the film, creating a surface of increased carbon purity.

The breaking of the C-C bonds is seen through the physical loss of thickness; the photoresist layer is far too amorphous to be utilized as a stable platform and the off-gassing of the oxygen and hydrogen leads to a thinner film. The pyrolysis procedure balances the need for a low oxygen-to-carbon ratio (the less oxygen, the purer the carbon surface) as well as suitable thickness. The purity of the carbon has been correlated directly to the temperature of which the pyrolysis peaks. The upper limit of this, however, is seen with a diminishing return on the ratio of oxygen to carbon. The ratio of oxygen-to-carbon at 1000^{o}C is found to be about 0.05, with little improvement thereafter. Coupled with the operating limitations of the quartz tube, furnace, and sled materials that hold the material, 1000^{o}C is set as the peak temperature for the procedure. [24]

The other variable in the pyrolysis procedure is the gas used for rendering the environment inert. The procedure can be done with forming gas (a mixture of hydrogen and nitrogen, used in metallurgical heat treating processes), pure nitrogen, or under a vacuum. Trials run with forming gas found a surface reaction occurs between the hydrogen and carbon surface at temperatures above 800^{o}C, which rules it out as a prospective material. A vacuum, while producing the purest of carbon surfaces, is by far the most delicate and exotic in terms of set up and use, as the amount of off-gassing that will occur is unknown. Nitrogen is the only reasonable material, and is readily available at a low cost.

It has been determined that, before the pyrolysis procedure, the surface in nearly uniform in terms of thickness and density. This uniformity decreases with the amount f photoresist applied; due to the interlaminar friction force of photoresist layers is lower than that between the bare silicon surface and the photoresist. However, the amount f photoresist needed to produce significant topographical changes is much more than will be used for these films.

2.5 C-MEMS

Carbon-based microelectromechanical systems (C-MEMS) are devices created in the same fashion as integrated circuitry. By repeating the sequences of fabrication (photolithography, etching, deposition),

[22] (A. M. Lyons, 1985)
[23] (Dr. Olivier J. A. Schueller, 1996)
[24] (Ranganathan, 2000)

silicon-based structure can be created on a very small scale. These systems typically have moving parts, as well as being electrically active, and have promise in a biological application. These C-MEMS can be easily replicated with features ranging from millimeters to micrometers, with photolithography able to produce features less than 100 nm in size; these techniques have produced MEMS devices and components such as valves, membranes, sensors, rotors, cantilevers and pumps. In order to make these systems biocompatible, they must be aseptically fabricated and hermetically sealed, as well as be made of biocompatible materials. The hope is to use the manufacturability and reproducibility from the microelectronics industry to replace other types of implantable systems, as well as to break new ground for implants to be used in: retinal correction, neural stimulation and microneedles all exploit the unique property set of MEMS (optical, electrical and magnetic sensitivity, small scale, quick functioning time) in a biological use. At current, they can be separated into the categories of implantable devices, inject able devices, or actuation systems.

2.5.1 C-MEMS Systems and Applications

One main implantable solution that requires biocompatible C-MEMS is that of a drug delivery system (DDS). Current polymer-based solutions are used, but are hindered by their lack of direct controllability; common DDSs are made of a polymer engineered to degrade at a certain rate under certain conditions (the characteristics of the site of interest) to release a certain, predefined dosage of a drug. MEMS, generally smaller, can be manufactured to respond to various stimuli, is it change in pH, temperature, concentrations of various solutes, or electromagnetic radiation. This, in conjunction with external digital controls and the quick response time of the MEMS system, makes and ideal platform for the distribution of potent drugs, be it hormones, growth factors, or other medicines that may harm the body if not targeted precisely enough. These C-MEMS can be fabricated to simply act as a reservoir for microparticles. This device can be used to diffuse the particles at a pre-determined rate (have a slow-dissolving cap made of glucose or starch, or a gold membrane which can be electrochemically dissolved when an anodic voltage is put across it), to a more complex device that can hold various dosages of different drugs which will release the correct amount based on its physiological surroundings or remotely via electrical control. MEMS, due to their potential complexity and controllability, are an attractive solution, despite their relative infancy in development.[25,26]

Injectable MEMS are researched to understand the feasibility of delivering other devices. One such system that has been developed is a C-MEMS carrier module that can deliver other C-MEM devices to the brain or places of tissue damage for electrical stimulation for tissue conditioning and regeneration, with the C-MEMS packaging using RFID tagging to be traced, identified and even controlled.

Actuating C-MEMS devices are devices in which the MEMS device actively engages in a biological task for a long period of time. One example is a pacemaker; while nearly 40 years old, the pacemaker is a beacon of synthesis between medicine and engineering to create a device that is one of the few implantable devices hailed as truly biologically integrated, being controllable, reliable, have active sensing and biological feedback. C-MEMS have the ability to target a diagnosed problem and act upon it

[25] (A. Desai, 1997)
[26] (A. Ahmed, 2002)

independently, leaving other cardiovascular functions untouched, unlike larger systems. The use of small machines inside the body to move mechanically opens up vast possibilities for medicine to work on a patient from the inside out, decreasing the need for invasive surgery.[27]

2.5.2 C-MEMS Biocompatibility

The most important factor of biologically-designed C-MEMS is that of biocompatibility; what the C-MEMS surface chemistry will do to the body, en-route to the area of need as well as at the site, and what the body with do the C-MEMS device. This realm of study is known as pharmacokinetics, and has been studied substantially due to the increased use of synthetic products in internal medicine, as well as the decreasing size of this technology.

Due to the very small scale of the C-MEMS components, any attack or modification to a surface could change the physical properties of the device to not work; cantilever beams can be eaten away which could lead to overstressing a part, or a surface can be modified in such a way it can no longer interact with the environment is was meant for. This "bio-fouling" largely consists of the adsorption of peptides and proteins that cells require, which can lead to a device being inhibited by cells adhering to the surface. There is a fine line that needs to be tread between biocompatibility and functionality; solutions have been proposed (such as coating the C-MEMS with a surface immobilized polymer: the most widely known and used is PEG, known to inhibit bio-molecular adsorption, and have it be released when the site for action has been reached), but the more complex C-MEMS that have been engineered to have certain physical properties (roughness, hardness, patterning) can be debilitated by the slightest of bio-fouling.

As the fabrication of the unit is mainly on a silicon wafer, research has been done to compare and contrast various silicon materials; single crystal silicon, polycrystalline silicon, silicon dioxide, silicon carbides and silicon nitrides. While SU-8 does leach nonvolatile residues in aqueous physiochemical solutions, most materials were found to be suitable when inside the body. [33]

2.6 Magnetite (Fe_3O_4) Nanoparticles

2.6.1 Biological Applications

From previous research, thin plain-carbon films manufactured by spin-coating S1813 epoxy on Si wafers are viable substrates for neuron growth.[28] Most neurons are electro-active; their growth is affected by electrical stimuli; the variables that affect dendrite length, adhesion, and rate of differentiation are not limited to just physical and chemical characteristics, but include the electromagnetic properties. To investigate this, we have selected magnetite nanoparticles to use in the fabrication of the carbon film by doping the S1813 epoxy before spin coating.

Magnetite nanoparticles are small particles (5-150 nm diameter) of Fe_3O_4, and have been the key focal point of research in fields such as micro-scale optics, electronics and biological systems. While speculated to be the oldest of all magnetic material, magnetite has been used most recently is

[27] (Grayson, 2004)
[28] (Pampuro, 2009)

microscale devices, be it as a ferrofluid (magnetite nanoparticles suspended in an organic solution, often toluene) or as a coating. In biological fields especially, much research has been focused on controlling the size, shape, and dispersability of these particles, characterizing the nanoparticles' ability to be used in certain biological situations.[29,30]

Magnetite nanoparticles, due to their alluring properties, have been researched in various biological applications. The high surface energy and large specific surface area of magnetite nanoparticles have been used for cell immobilization; microbial cells, when immobilized, can be, and are frequently, used in bioconversions, biotransformation and biosynthesis processes as they can be more readily reused and often yield better results than untethered cells in the biological process. By exposing microbial cells to a solution of magnetite nanoparticles, the particles were adsorbed onto the cell surface, but no deeper due to the physical properties of the particles. Once coated, a magnetic field was created and was able to immobilize the cells, and has proven to be an alternative to other immobilization methods, which run into issue regarding equal dispersion and mass transfer.

Magnetite nanoparticles have been utilized in medicine as an indicator and therapeutic solution for dealing with cancerous tumors in living creatures. The nanoparticles can be delivered to the malignant tumor through proprietary drug delivery systems. Once the nanoparticles accumulate in the cancerous cell tissue, it can be easily tagged and seen with conventional MRI techniques.[31] As the particles are biocompatible, they are not rejected nor cause adverse affects in the body. Their size, surface energy and charge affect the distribution within the region they target, but, once latched into the cell membrane of rapidly-splitting cancer cells, they will remain embedded into the cell wall, traveling with the newly-formed cancer cells.

More importantly, magnetic nanoparticles can be utilized in a cancer therapy known as hyperthermia. The process utilizes the region-specific nature of the delivery, as well as the ability for the nanoparticles to embed themselves into the cell wall, and not into the cell itself, causing abnormal behavior. When exposed to AFM, the nanoparticles, under an alternating magnetic field, will essentially vibrate, which can cause the destruction of cancerous tissue by the mechanical vibration of the particles. As this vibration will cause friction between cells, it will subsequently heat that region inside the body; this can signal the host's own immune system will target this area as well. This has been tested and demonstrated, and has been hailed as a solution that will greatly increase the quality of life for cancer patients during treatment.[32,33]

As our surfaces are intended for biological use, be it a staging surface for transplant or a platform for a biosensor that needs to be magnetically active, there has been use of magnetite nanoparticles in tissue engineering. The use of magnetically active nanoparticles in conjunction with standard keratinocyte (epidermal cell) growth was seen to improve the quality and the rate of cell growth, especially when

[29] (Ling Zhang, 2006)
[30] (Rochelle M. Cornell., 2003)
[31] (L.X. Tiefenauer, 1996)
[32] (Akira Ito, 2005)
[33] (P. Moroz, 2002)

subjected to a magnetic field. In addition, keratinocyte cells, once tagged with the particles, can be manipulated by magnets, stratifying them and forming a sheet when in the presence of a magnetic field, greatly improving the quality and ease of grafting of the cells.[34] Other uses, like this one, exploit the ability of the nanoparticles to embed themselves within the cell wall and not interfere with normal cell behavior.

2.6.2 Toxicity of Magnetite (Fe_3O_4)

While the magnetic nanoparticles may act as a catalyst for complex carbon surfaces to emerge from the pyrolysis procedure, they are not spent, broken down, melted, or otherwise lost, as they remain in the thinner carbon surface that is then used as a substrate for neuron culture. While their location in the our film has not been explicitly determined, it is assumed that, due to the large concentration we are using, there will be magnetite nanoparticles exposed on the surface. While carbon is benign to neuron cells, the presence of Fe3O4 calls into question the toxicity of magnetite to the PC-12 cells we are trying to culture.

Cytotoxicity, the quality of being toxic to cells, is a term given to various substances that adversely affect a cell. Treating a cell with a cytotoxic compound (in the form of presence in the same culturing media, injection, absorption/uptake, etc) will lead to the death of the cell, or to abnormal cellular behavior. The most common form of cell death is necrosis, where the cellular membrane loses integrity (collapses, bursts, or disintegrates) which compromises the vitality of the cell. Apoptosis is a cellular death where the cell membrane remains intact, and the death, as opposed to necrosis, has little physical impact on the cell. A process of programmed cell death (PCD), a cell will die via apoptosis when a biological trigger is tripped, be it the introduction of a malicious substance or presence in a foreign environment, and a domino effect of cell morphologies (cell shrinkage, nuclear fragmentation, chromatin condensation and ultimately DNA fragmentation) that lead to cell death occur. Apoptosis can occur when a cell is damaged beyond repair, is infected with a virus, or is in an unfavorable environment.

Biocompatibility and toxicity of magnetic microspheres are determined by many factors, primarily the magnetically responsive components[35], and the size of the particles, their matrix substance and the coatings used. [36] According to clinical trials, superparamagnetic iron oxide was tested to determine the pharmacokinetics (distribution, metabolism, bioavailability, excretion) and toxicity (acute and subacute toxicity, mutagenicity) of the particles, as they are to be used as a contrast for magnetic resonance imaging, MRI. The trials found that the iron oxide was fully biocompatible, with no toxic effects and little retention in the body, with concentration half-life's less than four days. [37]

Other sources[38] indicate that microspheres (a radius on the order of $1x10^{-6}$ m) that contained 30% magnetite by weight did have toxic effects on rats that were injected with a solution and let to incubate for 24 hours. In this case, the size and concentration of spheres were found to cause the abnormal

[34] (Ito, 2004)
[35] Magnetite, iron, nickel, cobalt, neodymium-iron-boron or samarium-cobalt
[36] (Hafeli, April 1999)
[37] (R. Weissleder, 1989).
[38] (Hafeli, April 1999)

cellular growth, though the toxic effects were not due to iron being leached into the system. As magnetite, as well as other iron oxides are highly stable, the amount of ionic iron (Fe^{2+} or Fe^{3+}) is highly unlikely, and will not interrupt or modify cell growth. From this, it does not appear that any iron will leach from our iron oxide nanoparticles into the system, disrupting cell growth.

While the body can handle and adapt to prepared samples, we must look at the interaction between raw magnetite and neuron cells. A 2007 study of magnetic nanoparticles (MNP's) by scholars at the University of California, San Diego, found that intracellular delivery of iron oxide, Fe_2O_3, had adverse affects on the ability for PC-12 cells to extend neurites in response to the presence of NGF. Their research goals were to see the toxic effects of iron oxide, in vivo, as "little work has focused on quantifying the effects that Fe_2O_3 internalization has upon cell behavior and, in particular, the ability of cells to appropriately respond to biological cues". The region-specific delivery of these nanoparticles is key to future drug delivery systems, as well as targeted use of magnetic hyperthermia and cell tracking through high-resolution MRI,[39] but the toxic effects need to be analyzed with closer detail.

This team determined that the increased concentration of Fe_2O_3 lead to a decreased number of neurites per cell (from a control of ~2.9 neurites per cell to ~0.9 neurites per cell in a 15 mM solution) as well as a decreased intercellular contact points per cell (where the PC12 cells connect to each other), from about 1 per cell in the control to a diminished 0.1 points of contact in the 15 mM concentration. The cells that were exposed to MNP failed to develop the same growth over the same period of time, at a standard density, that the control cells were able to. This retardation in growth is also coupled with cytoskeletal abnormalities, as well as less overall branching of neurites, which is crucial to the formation of neuromuscular connections as well as rate of regeneration, two key factors in using a nanoparticles-doped surface as a site for reparative neuron cell staging.[40] Despite these results, two things greatly differ from our experimentation. First, this test was done with free-floating nanoparticles in solution, whereas ours are fixed to the surface. Second, while Fe_2O_3 and Fe_3O_4 are both iron oxides, they vary in both physical and chemical properties.

A small team out of the University of Glasgow underwent research to further understand the influence of particles used in current medical practices (magnetic hyperthermia, imaging, cell tracking, etc) have on cells in culture. The world of medicine uses particles whose hydrodynamic size range from 10 nm to 500 nm, and have a variety of coatings, namely dextran, with others such as starch, albumin, silicone and polyethylene glycol (PEG). Our particles are not coated, as they are free floating in a toluene suspension and will not need to survive a journey to the targeted area inside the body. In this study, 8nm nominal diameter (between 7-15 nm) magnetite nanoparticles were used to create four different trials: untreated cells, staurosporin-treated cells, cells incubated with dextran-covered nanoparticles and cells incubated with plain, uncoated nanoparticles, very similar to the Fe_3O_4 that we are using. From the assays performed, a few useful tidbits were gleaned. First, the cells cultured with uncoated, plain nanoparticles had approximately 10% of the cells die due to apoptosis, whereas the control saw no apoptotic death, though the dextran coated saw roughly 20% and the staurosporin roughly 85% of the

[39] (Kircher MF, 2002)
[40] (Pisanic, 2007)

cells perish in the same manner. Cell death can happen in many ways, the typical causes being necrosis (physical cell damage) or apoptosis, a "programmed death" that the cell decides to undergo for various reasons. While this shows that bare nanoparticles may indeed be toxic, it still depends on the fact that the cells are mobile in the media while incubating, which is not valid in our experimentation, as they are fixed to the surface. [41]Further reading on toxicity due to particle uptake can be found elsewhere, and is out of the scope of this paper's topic[42]

2.7 Surface characterization

The physical, chemical, and electromagnetic properties of a surface will affect various aspects of cell culturing. The materials fabricated within this project will to be analyzed in order to seek correlations between these properties and cell growth, adhesion, and survival on the surface we culture them on. Of the measurable characteristics, we will be assessing surface energy, roughness (via AFM), electrochemical properties (through cyclic Voltammetery), and topological surface characteristics (via SEM). Other characterizations, such as hardness and electrical resistivity, are quite telling of the properties, but are unable to be measured for this project due to lack of available equipment. These procedures can be found appended to this report.

2.7.1 Surface Energy

The energy of a surface is a characteristic which may correlate to neuron-surface interactions we are studying. The test is done by placing a droplet of various substances on the surface and investigating the angle at which the droplet maintains with the surface. A flatter contact angle indicates a higher surface energy, as the droplet's shape is determined by the ratio between the fluid's surface tension at the fluid(variable)-gas(air) interface and the force of the interaction between the fluid (variable) and the surface (carbon film).

To analyze, the flatter the droplet is, the stronger the surface energy is. If there is little surface energy, (little affinity between the surface and the droplet), the droplet will have a high contact angle, as the surface tension will contract the fluid; if there is no affinity, the fluid will be a sphere. With a very high surface energy (large affinity between the surface and the fluid, a wet table situation), the surface pulls the fluid, and the surface tension of the fluid cannot contract the fluid into a more spherical shape.

To determine the qualitative angle into a quantitative energy is that of Young's equation. It is used to describe the balance of energies controlling the contact angle of the liquid drop on such a surface (equation 1). Furthur work done by Dupre indicated that thermodynamic work could be used to describe the energy involved with adhesion, in which is the reversible work done is correlated to the separation of unit area of solid/liquid interface. Combining these two, the Young-Dupre equation was formed as shown in equation 3.

$$\gamma_S = \gamma_{SL} + \gamma_L cos\theta$$

Equation 1: Young's Equation

[41] (C.C. Berry, 2004)
[42] (Zhang, 2002)

$$W_{ad}=\gamma_S+\gamma_L-\gamma_{SL}$$

Equation 2: Dupre Equation

$$W_{ad}=(1+cos\theta)$$

Equation 3: Young-Dupre Equation

Dispersion (gamma d), polar (gamma p) and hydrogen bond (gamma h) are the three different intermolecular forces that contribute to the calculation of total surface energy. Normally, the polar and hydrogen bond forces are encompassed in a single term (gamma p). Therefore, in order to derive the total surface energy, two liquids are needed and the sum of the two different intermolecular force terms will allow us to derive the total surface energy of the substrate.

2.7.2 Roughness

The roughness of a surface on this scale can be measured using atomic force microscopy (AFM). By measuring the resistance a single-beam cantilever that is pushed across the surface, the variations in height can be measured, and correlated to an overall roughness. If contact needs to be avoided, a non-contact optical profiler can be utilized to gain the roughness data.

Atomic Force Microscopy (AFM) is a non-optical method of microscopy, with the first atomic force microscope built in 1986 by IBM Research in Zurich; it was built off of the scanning tunneling microscope, developed in the early 1980's at the same facility, which won the creators, Gerd Binning and Heinrich Roher a Nobel Prize in Physics. The AFM was designed to overcome the constraint that the STM had; the samples themselves needed to be conductive. The AFM was designed to use the changes in atomic forces between a measurement apparatus and the surface to gain quantitative data. The AFM found in the Gateway Park facility at WPI is deployed by Asylum Research, and utilizes a MFP-3D-BIO AFM hooked up to a computer for image relay and interpretation.

The AFM is centered around the cantilever; as small, curved pieces of silicon or silicon nitride that has a small probe at the end, generally conical that is about 100 µm in width and 30 µm long. Various probes can be acquired and used, based on the application or sensitivity/characteristics of the material being analyzed. The AFM can be used for a wide variety of measurements; bonding and Van der Waals forces, electrostatic forces, capillary forces, roughness, and mechanical contact forces. In order to measure the displacement of the probe as it scans the surfaces, a laser is pointed at the cantilever, which naturally reflects off of the silicon and is captured by a photodetector. In essence, the cantilever will bend when subjected to the forces the surface applies to it, and this displacement will change the angle of the laser's reflection, thus generating an image with the height known over a specific location, x,y, on the surface. Scanned back and forth at varying speeds, with data sampled at various rates (measured in Hz), a surface image can be produced.

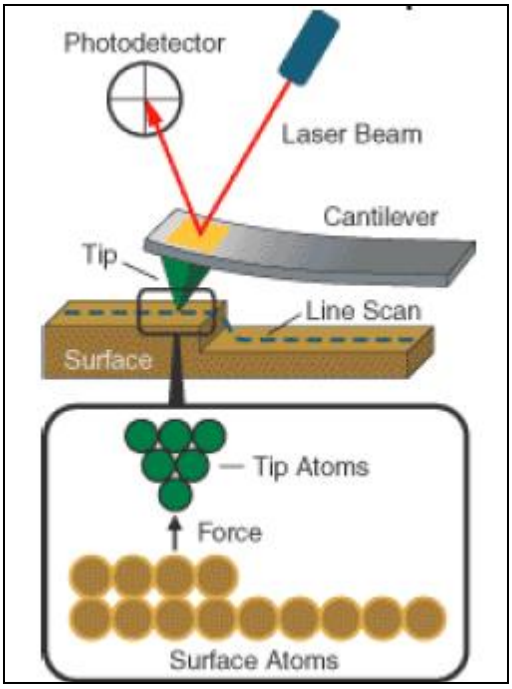

Figure 2: A basic diagram of the main components of the AFM during the scanning of a sample material.

An AFM can be used in two typical "modes": static (contact) modes and dynamic (non-contact) modes. The contact mode, as the name implies, has the tip come into physical contact with the material. However, this is not done at a standard height; this could cause the tip to, while scanning the surface, catch on the material (if it is not perfectly flat, which is very rarely the case) and snap the probe. Additionally, if the probe is brought too close to the surface, the attractive forces between the probe and the material will be strong enough for the tip to "snap in" and make contact. The sample, mounted on a small piezoelectric tube, can be raised and lowered in real-time with the motion of the cantilever; this allows for the probe to put constant force onto the material, and, couple with a very stiff cantilever, the resultant forces can be measured and then turned into the data one is looking to acquire.

A development in AFM microscopy has been the use of "tapping" mode, in which there is no contact with the AFM probe and the surface itself. The cantilever is oscillated at its resonance frequency with a small piezoelectric element; this causes the probe to oscillate with an amplitude of 100 to 200 nm. When the probe comes close to the surface, the amplitude of the oscillation will decrease, as the material has atomic forces that repel the probe from coming any closer to the material. The images extracted from this type of analysis are made by mapping the force the probe experiences due to the surface.[43]

The AFM was utilized for this project to determine the roughness of our samples. This factor is not only important to see if there are differences between the samples made with varying concentrations of the magnetite nanoparticles, but also due to the fact that is has been proven that neuronal cells are influenced by roughness. A 2002 study cultured nigral cells (collected from the subthalmus of prenatal

[43] (Baselt, 1993)

Wister rats) on silicon wafers which they had etched in grid-like patterns. The channels, etched out, varied in roughness, with the surfaces having less than a RMS roughness of 10 nm. From the results, the cells adhered and survived best on surfaces with an RMS roughness between 20 and 50 nm, with cell adhesion on surfaces below 10 nm and above 70 nm negatively affected by the roughness.[44]

SU-8 photoresist, widely used for the fabrication of high-aspect ratio microstructures (where one length dimension is an order of magnitude, or more, than the other; in this case, the fabrication of long, thin structures are desired), has undergone experimentation to see how surface roughness changes with different lithographic techniques. An AFM is utilized to calculate the roughness of not only the surface, but the sidewall of 500 µm-tall structures, as this is vital to integration with the rest of the C-MEMS application.

If surface roughness is proven to be a vital characteristic in the growth of neurons (neurons being attracted to grow in topographical wells as opposed to the peaks and valleys of surface energy), a rougher medium can be used to coat. The use of spray coating in the fabrication of C-MEMS and packaging has been developed to fabricate platforms that require non-planar surfaces; senor and actuator devices, used for measuring pressure and acceleration as well as micro-lens and mirror apparatuses, require a platform with severe topography in which spin coating will not be practical. Using S1813, French scientists utilized spray coating equipment to fabricate C-MEMS systems with non-planar elements with success.

2.7.3 Cyclic Voltammetry

A material's surface needs to be characterized to ensure the surface properties, both chemical and physical, are as desired. For our work, the characterization is used to correlate cell morphology and growth patterns with the material's properties. Cyclic Voltammetery (CV) is used to characterize the surface by electrochemically surveying the surface's response to various electric potentials, and the change between them, in a standardized environment (ion solution). The voltage is applied to the surface, and the meter uses the changes in current, brought about by a varying electrical potential profile, to find when the reduction and oxidation occur in an electrochemical cell. The CV is a potentiostat using a three-electrode setting. The working electrode is set to a constant electric potential while the current in the counter electrode changes with respect to a reference electrode at a known potential. A very common reference electrode is Ag/AgCl with an E_o = 0.222V. The working electrode and the counter electrode create a potential difference, i.e. voltage. If they are connected through a conductive surface, the surface can be considered as conductive. The potential in the counter electrode ranges usually from -0.3 V to 0.7 V. When electric current passes through, a redox reaction occurs on the surface, which is induced by the solution in which the electrodes are soaked. Generally this solution is a $K_3[Fe(CN)_6]$ During the redox reaction a reduction potential can be detected through a Gaussian distribution whose peak is usually seen at 0.22 V The oxidation potential is detected at its maximum at 0.18 V. Steep peaks correlate with greater current requirement, i.e. better surface conductivity.

[44] (Y. W. Fan, 2002)

2.7.4 Surface Imaging (SEM)

The uses of optical characterization of materials is the most basic, but, as technology has advanced, the detail at which we can analyze a surface has increased exponentially. At current, scanning electron microscopy is one of the most powerful microscopy techniques available today. Originally developed in the 1950's, the SEM is used to study the surface of solid objects by bombarding them with a beam of electrons. When the beam hits, the electrons will be scattered, and can be seen as X-rays, Auger electrons, primary and secondary backscattered electrons, as well an induced specimen current and cathode-luminescence: this information is amassed and processed into an image.

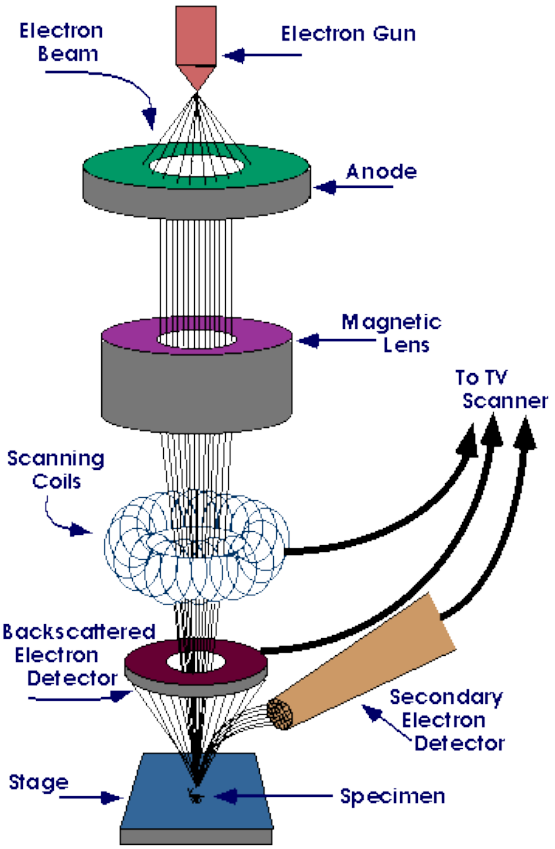

Figure 3: A simple diagram on the basic SEM inner workings[45]

From this, images with magnifications up to 500,000 times showing details less than 1 nm in size can be acquired. Samples must be prepared in a very certain way, to encourage the correct dispersion of electrons, and must be electrically conductive.[46]

[45] (Indiana State University, 2007)
[46] (Goldstein, 1992)

3 Materials

3.1 Cell Culture Chemicals

The two cell types require particular growth media for their maintenance and differentiation. Below is a brief explanation of most of the chemicals that have been used during the cell culture procedure and their purpose.

3.1.1 Phosphate Buffered Saline (PBS)

PBS is a buffer solution that maintains a constant physiological pH of 7. It is prepared in the laboratory in such a way that it forms an isotonic solution in which ion concentrations match to those inside the cells. PBS is prepared at a 10X stock concentration and diluted 10 times to bring it down to 1X. It is an essential solution for cell culture. Its most common role is to rinse petri dishes coated with cells.

3.1.2 DMEM

Dulbecco Modified Eagle's Medium is a type of growth medium patented by Invitrogen Inc. which is an essential product used in cell culture. It finds usage in most type of cells such as those of humans, monkeys, hamsters, rats, mice, chicken etc. The medium contains several aminoacids, salts, such as calcium chloride, sodium chloride, potassium chloride, magnesium sulphate, sodium phosphate etc., glucose, vitamins such as folic acid, nicotinamide, riboflavin, and B-12, iron, and most importantly what gives it the color is phenol sulphophthalein (PSP, also known as phenol red) which serves as a pH indicator. The red color corresponds to a physiologic pH, which includes values close to 8. The yellow color relates to the acidic environment of 6.6 or lower. The pink, fuchsia colors correspond to basic environments of 8.1 and higher.[47] Based on the cell type this media is grouped into Low Glucose DMEM and High Glucose DMEM. The choice of glucose is based on the type of cell used and on previous protocols.

3.1.3 Trypsin

Trypsin is an enzyme which participates in the cleavage of proteins through a hydrolysis reaction. Despite its preference for arginine (Arg, R) and lysine (Lys, L)[48] it cleaves peptide bonds between other aminoacids as well but not as efficiently and quickly. Trypsin is used in the laboratory to detach cells from surfaces. During cell culture the petri dishes used are made of a polystyrene polymer which is coated with some lysine-based chemical. The arginine groups on the cell's membrane have high affinity for lysine, allowing them to adhere within only few hours. However, for our experiments non-coated petri dishes were used to favor adhesion only with the carbon surfaces.

3.1.4 Nerve Growth Factor

The nerve growth factor (NGF) is a tertiary protein found in the target tissue of a signaling pathway in most neurons. These cells release NGF, which then binds to a receptor on the cell surface, TrkA, for which it has high affinity. Through the synaptic cleft it is transported into the axon of the motor neuron. As of today NGF is the only known neurotrophic factor that can be retrograde-transported from the axon to the soma. It is known to be necessary to promote neuronal differentiation as well as to mediate

[47] (Invitrogen, DMEM - Dulbecco Modified Eagle Medium, 2009)
[48] (Chang A., 2009)

survival and maintenance of the differentiated state of sympathetic and sensory neurons.[49] NGF was applied to PC-12 cells only since they represent a good model of undifferentiated neurons.

3.1.5 Poly-D-lysine

Poly-D-lysine is a protein whose monomer is the aminoacid lysine. It is a charged protein; therefore it is usually purchased as poly-d-lysine hydrobromide. HBr is used to neutralize the positively charged polypeptide and to solubilize it in water. Its common cell culture purpose is to coat glass surfaces so that charged cell membrane proteins can bind to the surface. This is a very common laboratory practice for cell adhesion experiments. Poly-d-lysine coated surfaces will be used as control throughout all the experiments.

3.1.6 DiI dye

DiI is one of the several lipophilic dyes available in biological applications, which is capable of penetrating through the cells' membranes allowing them to be visualized under the microscope. DiI traces the morphology of cells permitting a clear identification of their neurites. This dye is produced by Invitrogen and its IUPAC name is 1,1',di-octadecyl-3,3,3',3'-tetramethylindiocarbocyanine perchlorate. Being fluorescent, DiI is excited at a wavelength of 543nm in the green light region and emits at a higher wavelength of 560nm, which falls under the red light region. It fluoresces red in an RITC filter setting. The dye is usually diluted in ethanol because of its solubility and stability with this solvent, and especially because ethanol plays a very important role in the reaction occurring when the dye penetrates the cell membrane.

3.1.7 Mowiol Mounting Medium

Mowiol is a very viscous fluid used in laboratories when preparing cells for imaging under the microscope. The mounting medium is usually used to attach a cover slip to the cell surface of interest, preventing the cells from degrading and allowing the cover slip to fully adhere to the surface. It is usually left overnight and the day after, the samples are available for microscope testing.

3.2 Cell Culture Media

All cells behave differently based on the chemicals' type and their concentrations. Over the course of centuries optimal growth media have been developed, which are well-known and used during laboratory experiments with each type of cell available for purchase. The following list gives a brief display of the compounds used in the preparation of PC-12 cells along with their respective concentrations.

PC-12 Cell Culture Medium

- High glucose DMEM
- 10% (v/v) Horse Serum, a type of growth factor (protein) for PC-12
- 5% (v/v) Fetal Bovine Serum, a type of growth factor (protein) for PC-12
- 1X Penicillin/Streptomycin, an antibiotics' mixture to prevent bacterial growth due to occasional non-sterile practices.

[49] (T.P. Misko, 1987)

3.3 Material Fabrication Chemicals

3.3.1 S1813 Photoresist

For our substrate fabrication, we are using epoxy as a carbon precursor. There are a wide variety of epoxies; however, we are using a widely-known epoxy used in the manufacture of microelectronics, Shipley S-1813. The material, a very viscous polymer, is light sensitive, and is used in photolithography in industry. There are various characteristics photoresists have and are classified by: tone, developing light wavelength, chemical constituents all play into the various applications they can be used in.

The "tone" of a photoresist reflects how the material responds to UV radiation. A positive photoresist, when coated with a photoresist developer, will degrade under UV light. A negative photoresist, in contrast, will be insoluble to the photoresist developer. This is important with direct applications to photolithography: however, other physical processing properties are depended on the type of photoresist used. For example, positive photoresist will prove less able to adhere to silicon, whereas a negative photoresist has excellent adhesion. Negative photoresist is less expensive than positive resist, with each having different developer bases (positive using aqueous solutions, negatives using organic solutions). Additionally, the epoxies are typically based of PMMA, PMGI, phenolic formaydehyde (Novolac systems) or SU-8; each gives the material the chemical backbone, and make up the polymer backbone of the material. SU-8 is well know for its resilience to being stripped from the silicon base, despite the presence of a harsh acid and temperature environment.

Due to the lack of stability of SU-8 after pyrolysis[50], S-1813 was assessed. Though being positive, it proved, with the addition of the HMDS primer, to be very stable before and after the pyrolysis procedure, and accepted the nanoparticles solution without trouble. From the Shipley 1800-series photoresists, we can see that is does not need to be spun excessively fast to generate the thick coat needed, and is on-hand in our clean room. As it is a proprietary resin system, the chemical formula is not published, but it is made up of 71-76% propylene glycol monomethyl ether acetate, 10-20% mixed cresol novolac resin, 0.1-1% fluoroaliphatic polymer esters, and between 1-10% diazo photoactive compounds. [51]

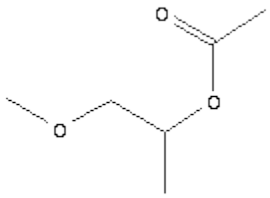

Figure 4: Structure of Propylene glycol monomethyl ether acetate, $C_6H_{12}O_3$

In the fabrication of C-MEMS, the carbon surface is patterned by standard photolithographic techniques. The non-patterned material is stripped away, leaving the desired part exposed. This stripping of SU-8 is

[50] (Pampuro, 2009)
[51] (Shipley, 1998)

commonly done by using hot NMP (1-methyl-2-pyrrolidinone), a polymer, or an oxygen-plasma. However, non-patterned surfaces to be used as a structural component, like the substrates we are investigating, will need to be separated from the silicon base in order to be used. Many materials have been described as workable as a sacrificial base layer. Electroplating the wafer base with a copper layer 5-10 microns thick has proven to be a practical material, though the rough copper surface is reflected in the surface of the carbon substrate. Other metals have been explored, including a thin film of 5/50/50 nm Cr/Au/Cr which has been used as a sacrificial layer to release 200 µm × 50 µm × 1.5 µm SU-8 cantilever beams. Other types of photoresists can release SU-8 structures smaller than 0.01 mm^2, and toluene-dissolved polystyrene has proven to be a material with laboratory-confirmed tests of its ability to release the SU-8 photoresist. [52]

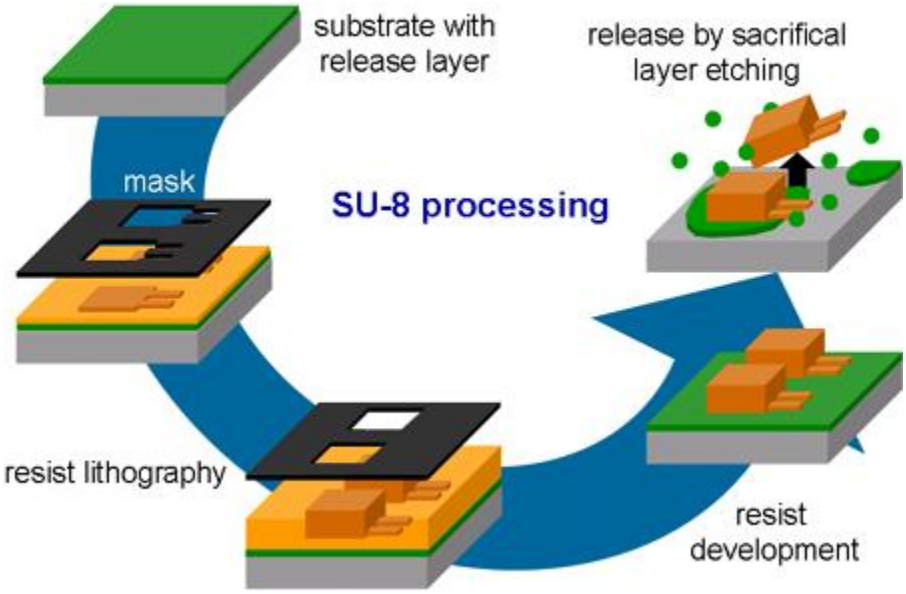

Figure 5: A graphical representation of SU-8 processing using photolithography

3.3.2 HMDS Primer

Hexamethyldisilazane (HMDS) is a compound with a molecular formula $((CH_3)_3Si)_2NH$. At room temperature it is a colorless liquid which has the ability to slowly hydrolyze in humid air. For this reason HMDS is handled using air-free techniques. Its main use is in dehydrated techniques in which perfect dryness is crucial, such as Scanning Electron Microscopy (SEM), Chromatography (GC, HPLC), Spectroscopy (NMR, IR, MS), photolithography, etc.

SEM requires the sample under analysis to be perfectly dry in order to correctly determine the surface structure. However, the drying of the material sometimes causes stress and deformation of the sample. HMDS can be used in this case in order to react with the water molecules and the oxygen in the air to produce three gases; ammonia, silicon dioxide, and hydrogen.

In GC and HPLC HMDS is used for deactivating and coating chromatographic supports. This silane can react with the surface making it inert, eliminating chances for polymers or other substances required for

[52] (Paik, 2002)

separation to elute from the column. On the other hand it eliminates surface moisture by making the surfaces lose their surface energy by becoming hydrophobic.

In photolithography, HMDS reacts with the hydroxyl groups formed during the inevitable oxidation of the silicon wafers. After the reaction terminates the chemical group remaining on the surface is methyl, which turns the surface hydrophobic. This is the preferred environment a negative photoresist requires. Below is a picture of the reaction process of an oxidized silicon wafer with HMDS.

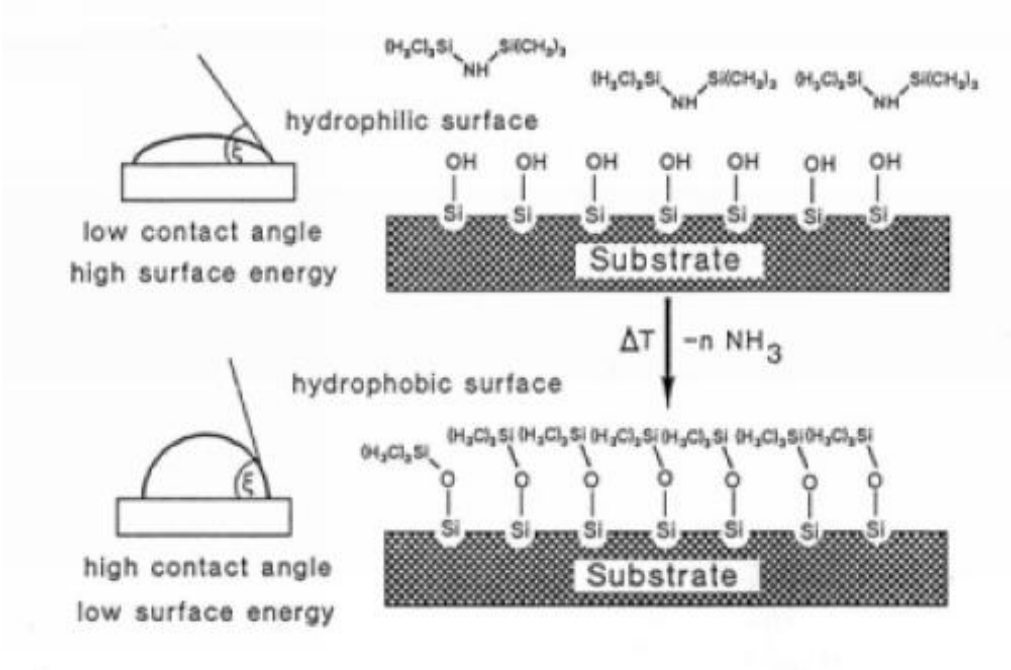

Figure 6: Reaction of the HMDS primer with the silicon surface

4 Methodology

4.1 Substrate Fabrication

4.1.1 Synthesis of Iron Oxide Nanoparticles

The magnetic nanoparticles (MNPs) were created by combining a mixture of FeO(OH), oleic acid and 1-octadecene was refluxed at 320 ºC for 1 h under nitrogen atmosphere. During this process, the solution changed its color from turbid black to black. The resulting MNPs were precipitated with acetone and collected by centrifuge at 4000g. After that, Fe_3O_4 MNPs were further purified by repeated extraction of the precipitate with $CHCl_3$/acetone (1:10) until a powder of Fe_3O_4 MNPs was obtained. The powder of Fe_3O_4 MNPs was stored at room temperature for further application. To create a solution, the nanoparticles were dissolved into toluene creating a black ferrofluid, responding to magnetic fields. The concentration of nanoparticles we used was very high, at 47.75 mg/mL, with the nanoparticles having a diameter ranging from 1.4 nm-10 nm.

4.1.2 Photoresist with Doped Nanoparticles Preparation

The nanoparticles, mixed in with the toluene, needed to be mixed into our SU1813 epoxy precursor in order to, ultimately, attain an uniform distribution of the MNPs in the surface. In order to give a decent spacing between concentrations, the trials were decided to be made up of four substrates. First, we would fabricate an unmodified S1813 photoresist, giving us a plain carbon surface which to compare with previous work; these samples are known as PC samples or #1 samples; no MNPs are added to the 8 mL of photoresist used per wafer in the spin coating procedure. In order to test the influence of the magnetite MNPs on the characteristics of the surface, three surfaces would be created with varying amounts of the MNPs. The lowest concentration mixes 200 µL of MNP solution into the 8 mL photoresist; the medium concentration uses 500 µL of MNP solution, and the highest concentration using 800 µL of solution. These are referred to as Fe_3O_4 0.2, Fe_3O_4 0.5 and Fe_3O_4 0.8, respectively, further truncated to sample types #2, #3, and #4, used for times where writing surfaces, i.e the bottom of 22x22 mm wafers and 25mm diameter petri dishes, were too small for legible clarification.

As the large store of MNPs are housed in Gateway park, 2 mL of nanoparticles solution were transported to the clean room in the basement of Higgins Labs, as well as 5 mL HMDS primer and four (4) mixing vials; these are used as a vessel to mix and store the 8 mL photoresist (housed in the clean room) with the nanoparticles before the spin coating procedure.

4.1.3 Spin Coating

The spin coating procedure is the process of which we take the liquid epoxy photoresist, doped with MNPs, and transfer it onto a 4 inch diameter silicon wafer, creating a very thin film of epoxy on said silicon wafer; the coating, approximately 10 µm in thickness, is then let sit for 48 hours (to dry) in a UV-protected area (to discourage decomposition) to be then further refined during pyrolysis. Due to the sensitive nature of surface impurities on thin films, all fabrication is done in WPI's level 10,00 clean room, found in the basement of Higgins Labs, adjacent to the Fluids laboratory. In order to appropriately use the clean room, direct supervision from Peter Hefti, a research fellow in the Mechanical Engineering

department was required, and proper clean-room setup was needed. This setup can be found in Appendix C.

The spin coating process begins with removing the silicon wafer from the storage container (wrapped in aluminum foil to prevent UV degradation) and rinsing the wafer in an acetone bath for two minutes. After being rinsed in acetone, the wafer is sonicated in methanol for an additional two minutes. These two processes are conducted to ensure the remove of all contaminates on the wafer surface. Following the sonication, the wafer is blown dry with nitrogen gas and placed in a flowing water bath for another two minutes.

After being cleaned in the water bath, the wafer is first blown dry with the nitrogen gas as after the acetone and methanol treatments. Additionally, the wafer is dried in the 110°C oven for one minute to complete remove all fluids from the wafer surface. The goal of the cleaning process is to ensure a smooth, contaminate-free surface for photoresist attachment. After removing the wafer from the oven, it is placed on a cooling rack to ensure the HMDS primer, the first coat, does not begin to be heated during the spin-coating; the HMDS is volatile, and any heat before or after its application will compromise the surface-photoresist adherence during the pyrolysis.

The silicon substrate, now cleaned, can be loaded into the spin coater. The bar must be lifted (by using the top actuating lever) to allow for space to load the wafer. By taking the wafer in tweezers, one loads the wafer into the center of the disc, ensuring that it is centered by lining up the curved edge of the wafer to the etched angle bracket. Once loaded, the second (lower) valve can be opened, creating vacuum between the disc and the wafer. The spin coater is set to spin at 3000 RPM for the duration of 90 seconds; once loaded, one must engage the drive an check the wafer to see if it is centered: the wafer will look unbalanced if not set correctly.

Once the wafer is set correctly on the disc, 1 mL of HMDS primer is added to the center of the wafer as quick as practical. Once done, the spin coater is engaged and spins for the set 90 seconds. From here, the first of four layers of photoresist is added. 8 mL of the photoresist are taken and transferred to one of the clearly labeled mixing aliquots brought over from Gateway. Then, the appropriate volume of nanoparticles are added and mixed. Once mixed, 2 mL are extracted from the mixing aliquot via two 1mL glass pipettes. The aliquot-to-surface transfer should take the least amount of time possible, to prevent any drying/stagnation of the liquid; such immobilization could lead to an uneven coating on the surface.

After the 90 seconds of spinning, the wafer is then transferred with tweezers to the oven, set at 110C for 90 seconds. From here, it is extracted, let to cool on the cooling rack, and loaded again, reciving the second of four layers. This is repeated until the 4^{th} layer is cooled; once done, a small identifier is etched, using the tweezers, to indicated which sample it is, be it PC (#1), or one of the nanoparticles doped samples (#2-4)

4.1.4 Pyrolysis

The pyrolysis procedure is carried out to reduce the thickness of the material down to two microns, while removing hydrogen and oxygen to create a more pure carbon material. After the prerequisite 48 hours of ageing, the wafers can be prepared for the pyrolysis procedure.

As we make four wafers each spin-coating session (one for each concentration), we will look to pyrolyze three of each, making twelve total samples. Each sample is to be 22x22 mm; to cut them to small squares, the wafer is taken and put epoxy-side down onto a clean cloth. The wafer is then scored with a diamond-tipped pen, using an aluminum cutting angle that is 22mm wide. To ensure straight cuts, the aluminum angle is aligned with the flat cut of the wafer (each wafer is "keyed" with a bit of one edge cut off) in one direction only. After scoring, the wafer is taken and placed over the edge of the table, aligning a scoring mark with the edge. Using a small bit of force, the wafer can be broken along the scored edge, and will result in long 22mm wide strips of material. From here, these can be further cut widthwise to get a 22x22mm square. Each square is then identified with a 1, 2, 3 or 4 with a permanent marker on the bottom of the wafer (silicon side).

Once cut, the pieces must be loaded onto trays. The trays have been cut from silicon or silicon dioxide wafers which had shown surface defects. The samples are loaded with the photoresisitve side facing up, with the bare, reflective side of the tray facing down. Three trays are used, with four sample per tray, and loaded in one by one into the quartz tube. The quartz tube has two ends, one with a small, L-shaped vent and the other with a flanged opening. The flanged opening, on the side of the tube that is clear (not darkened by carbon deposits from previous runs) can be unscrewed and removed in order to load trays. In order to rach, a metal wire has been fabricated, ith an L-shaped end, to push, ramrod-esque, down the tube. The heating elements in the furnace are most consistent in the center of the tube, and should be placed accordingly.

Once loaded, the gasket is screwed back on, and the quartz tube is loaded into the furnace bed. Once aligned, the tube that leads to the nitrogen (through a rotameter), the blue valve, can be connected. Hooked up, the nitrogen can then be turned on from the canister; when it is opened fully, the pressure regulator can then be opened up to the second hash mark, correlating to 10 psi. Then, the hood valve can be opened, and a flow should be registered by the rotameter (on the inside of the hood). This should be set to 100 SCCM to ensure excess nitrogen flow. The nitrogen should flow for 10 minutes before any heat is applied.

After ten minutes of nitrogen flow to ensure an inert environment, one can switch on the 40 amp fuse on the front of the Blue M furnace control. For this procedure, the maximum temperature is set to 1000°C. For the two step heat procedure, the initial heat rate must be set to 2°C/minute. This is done by holding down the blue button for 5 seconds until the options display appears and then pressing the blue button to cycle through the options until LoC (level of control) is displayed. Using the arrow keys, set LoC to -1 and then press the blue button repeatedly to cycle through the options until UPr (up rate) is reached. The arrow keys are used to adjust the heat rate to the desired value. For the initial heat rate, UPr will be set to 2. The blue button is then held down to return to the main menu. Once the furnace

reaches 300°C (displayed in the red letters on the display,), UPr is then changed to 10, and the furnace is left to reach 1000°C.

Once the furnace reaches 1000°C, the controller is turned off by flipping the switch used previously to turn it on and is left to cool for several hours with the gas still flowing. Once the furnace has reached room temperature (which may be confirmed by turning the furnace on for a brief period and observing the temperature reading), the tube may be removed from the furnace and the samples removed.

4.1.5 Poly-D-lysine coating

The control for the experiments using PC-12 consisted of poly-D-lysine coated cover slips. Several cover slips were precleaned in a 50:50 HCl solution in ethanol for several hours. Afterwards they were boiled in a furnace for 30 min in order to kill the remaining bacteria. The cover slips were rinsed in dH_2O and stored in dH_2O under the chemical hood until further use. A solution of poly-D-lysine in water was initially prepared at a concentration of 10µl/ml. In a 10 cm diameter dish we placed about 12 cover slips. 300µl of the diluted poly-D-lysine solution were placed on each cover slip and they were let to dry under the hood for about 3-4 hours. Then they were again rinsed with dH_2O to remove the unreacted products. A detailed sketch of the reaction mechanism for the poly-D-lysine coating is shown below.

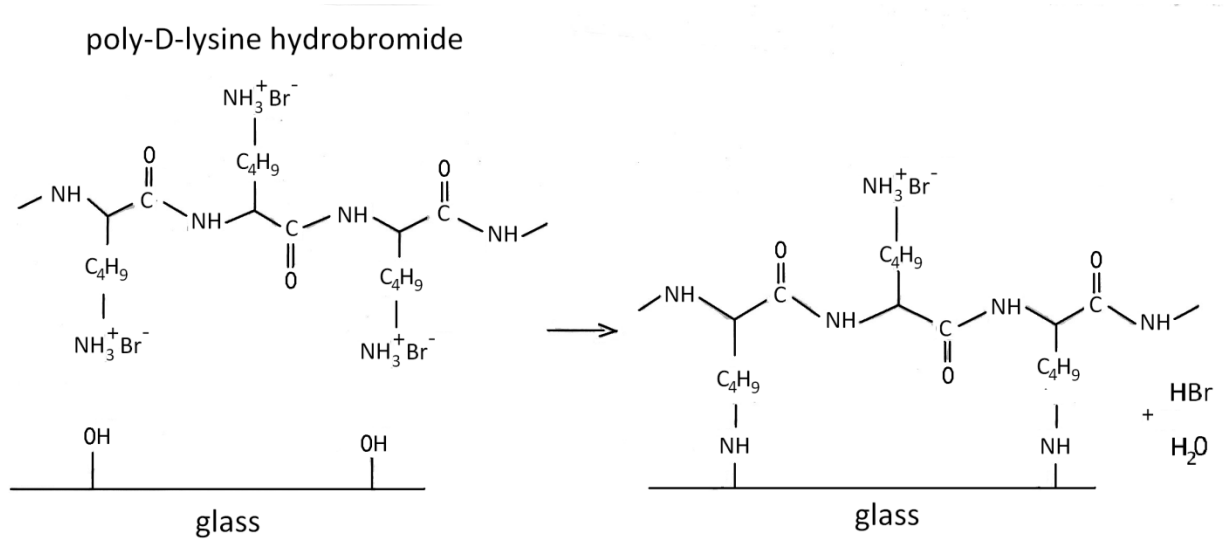

Figure 7: Mechanism of poly-D-lysine hydrobromide reaction with glass surface

4.2 Cell Preparation

As previously mentioned our group worked with the rat neuronal cell line known as PC-12. The technique that was utilized for its culture is explained in detail below. The purpose of these experiments was to test iron oxide doped carbon wafers at different concentrations vs. plain carbon coated wafers on PC-12 cells. Poly-D-lysine coated glass cover slips were set as the control. The two substrates were also tested whether they induce neuronal differentiation. Two sets of experiments were performed, one of which included NGF. The detailed experimental procedure is explained below.

4.2.1 PC-12 Culture on Substrates (without NGF addition)

Four types of carbon substrates were tested for cellular adhesion, proliferation, and differentiation. Three magnetite doped carbon substrates at 4.8 mg/ml, 3.0 mg/ml, and 1.2 mg/ml of nanoparticle solution were prepared along with one plain carbon substrate and one poly-D-lysine coated cover slip for PC-12 experimentation. The procedure was performed in triplicate.

The substrates were initially let to sterilize under UV light in the hood for 2 hours after being put into 35 mm diameter suspension cell culture dishes and labeled respectively. The suspension cell culture dishes are made of non-treated polystyrene material which prevents the cells from adhering to the surface but to our material. During this process the caps were made sure to be removed from the dishes in order for the sterilization to be more efficient. The samples were then rinsed 3 times with PBS to remove any debris. When determining the cell seeding concentration it was made sure that the number of cells per unit area was constant for all surfaces, given that the cells deposit on the bottom of the plate. This number was taken from the datasheet catalog for the transfection procedure using Lipofectamine 2000 from Invitrogen's website.[53] Our calculations were based on a cell number of $5*10^5$ cells/dish for a 35 mm diameter plate and a 2 ml volume per dish. The area of each 35 mm diameter dish is about 10 cm^2. Therefore our goal was to obtain $5*10^4$ cells/cm^2. The area of interest for our wafer is about 5 cm^2 (2.2 cm x 2.2 cm). Hence, the number of cells was calculated to be $25*10^4$ cells/wafer.

Calculations and measurements of cell seeding concentration:

The confluent 10 cm diameter dish used for our experiment was undergone a set of procedures to detach the cells, in order to transfer them to the wafers. Using sterile techniques the old growth medium was aspirated out and the dish was slowly rinsed once with PBS. 5 ml of new growth medium was added to the dish which was continuously pipetted up and down within the dish for about 30 min so that only a few cells would remain attached. The volume was stabilized to 10 ml by adding extra fresh growth medium. The cell number per unit volume was determined using the microscope. We counted the amount of cells in the confluent dish twice. The results were $127*10^4$ cells/ml and $115*10^4$ cells/ml. Taking the average we used $121*10^4$ cells/ml of concentrated stock cell solution. To obtain $25*10^4$ cells/wafer, then we were required to use 0.223 ml of stock cell solution. To completely cover the wafers, a total volume of 3 ml was required. This was done by adding an extra 2.777 ml of growth medium. A slightly different calculation was required for the poly-D-lysine cover slips since their surface area was about 1.5 times as small compared to the carbon wafers. A different confluent dish was used for them, hence a different stock cell concentration. The detailed calculation is shown in section 4.2.3. The main assumption for all these calculations is that no cells died or were lost throughout the experiment. To prove this assumption another experiment was performed, which is discussed in section 4.2.3. After the calculated amounts were added, the dishes were incubated at 37 C overnight. Two days later, the samples were prepared for imaging.

Staining for microscope scoring:

[53] (Invitrogen, LipofectamineTM 2000, 2002)

Two days later the cells were ready to be fixed. Fixation refers to the treatment of the material so that all the cell processes come to a halt without destroying the cellular structure. The growth media in all the plates was aspirated out and enough paraformaldehyde solution (4% in water) was added to cover the substrates. During this procedure it was made sure that it was worked with one plate at a time so that the samples do not dry out. The purpose of paraformaldehyde is to fix the cells, i.e. to stop the cell's life cycle so that no more cell growth/differentiation will occur. The samples were soaked in paraformaldehyde for 5 min. In the meantime the DiI solution was prepared by diluting the concentrated dye (1 mg/ml) 1000X in pure ethanol 200 proof. A total volume of 2 ml was prepared which was transferred equally into two separate 1.5 ml microfuge tubes. The aliquots remained wrapped in aluminum foil at all times and in an ice bucket to prevent light and heat from degrading the protein. After 5 min the paraformaldehyde was removed and the substrates were rinsed 3 times with PBS. Each sample consecutively followed a set of procedures for staining purposes. The substrates were dried by making sure the cells were not disturbed. Then the DiI solution was applied by adding 20µl drops for about 1 min. To remove the excess dye the samples were rinsed once with PBS. They were once again dried out and 60µl of Mowiol mounting medium was added to the substrates after they were placed on a paper towel. The pre-labeled microscope slides were slowly put on top of the respective substrates making sure that no air bubbles were trapped between the two surfaces. The samples were then let to dry overnight. The following day a set of pictures were taken using a 40X lens magnification. The data were then analyzed by measuring all the neurites' lengths in each picture.

4.2.2 PC-12 Culture on Substrates (with NGF)

This procedure is very similar to the non-NGF experiment with the only exception that one day after the cells are seeded, NGF is applied. More specifically, the substrates were sterilized under UV light in the hood for 2 hours after being placed in 35 mm diameter suspension cell culture dishes and labeled respectively. After sterilization the samples were rinsed 3 times with PBS. The confluent PC-12 dish was pipetted continuously and vigorously to detach as many cells from the surface as possible. Their concentration was determined using a Neubauer slide. The number of cells per unit area was kept constant at $5*10^4$ cells/cm^2. Since our wafers were approximately 5 cm^2, the total number of cells was calculated to be $25*10^4$ cells/wafer. A more detailed process has been shown in the calculations and measurements of cell seeding concentration for the non-NGF PC-12 culture section. To determine the cell number per unit volume, the counting chamber was used. The calculations are the same as those in section 4.2.1.3 since the same batch of cells was used. After the cells were added respectively onto each sample, they were let to seed overnight. 24 hours later a 0.1 mg/ml NGF solution was diluted 1000X with growth media in the following fashion. Having a total of 15 dishes (5 types repeated 3 times) containing 3 ml of growth media each, required a total of 45 ml PC-12 growth media. In a 50 ml centrifuge tube added 45 ml growth media and 45 µl NGF solution, diluting it therefore by 1000X. The tube was shaken vigorously to obtain perfect mixing while avoiding bubble formation and protein degradation. The old growth media onto each sample was aspirated out and 3 ml of the prepared NGF growth media solution was added onto each dish. The cells were left overnight to react and the following day they were prepared for imaging. To avoid being repetitive, the procedure that follows corresponds to "Staining for microscope scoring" in section 4.2.1.

4.2.3 Cellular Adhesion Test

When the media is removed from the material, being it for preparation for fixation, being it for preparation for NGF addition, it was impossible to know if all cells that were seeded were not aspirated out but attached to the substrates 100%. The reasoning behind this experiment came from the fact that the cells might not have had enough propensity to adhere, causing some of them to die and float in the medium or precipitate on the sides of the plates. To make sure that the results obtained from the experiments would be comparable for all types of substrates, we measured the cell concentration one day after they were seeded. Within one day the cells should adhere and little to no proliferation should occur. Five plates containing 1.2 mg/ml Fe3O4, 3.0 mg/ml Fe3O4, 4.8 mg/ml Fe3O4, plain carbon, and poly-D-lysine cover slips were prepared for testing. On day 0, we counted the amount of cells in the confluent dish twice. The results were $129*10^4$ cells/ml and $148*10^4$ cells/ml. Taking the average we used $138.5*10^4$ cells/ml of concentrated stock cell solution. The final seeding concentration for the carbon-based substrates was $9*10^4$ cells/ml. Therefore the amount of stock cell solution used was 0.180 ml along with 2.820 ml medium to obtain a final volume of 3 ml. Since the the poly-D-lysine cover slips were 1.5 times as less in surface area, their concentration needed to be $6*10^4$ cells/ml. To obtain $6*10^4$ cells/ml a volume of the stock cell solution of 0.09 ml was required and 1.909 ml PC-12 medium for a final volume of 2 ml. The cells were let to adhere overnight. On day 1, the media was aspirated out and the cells were treated with 0.5 ml trypsin solution. They were let to sit in trypsin solution for 10 min to allow cells to detach. Then the trypsin-cell solution was mixed vigorously for another 3 min using a pipette. Another 0.5 ml medium was added. The solution was mixed and its concentration was measured using a Neubauer slide, a counting chamber which allows for a fairly accurate cell counting.

4.3 Film Characterization

4.3.1 Roughness: AFM

The AFM was operated by graduate student Sena Ada, who is certified to use the equipment. The samples we wanted to have tested were selected, looking for the most optimal surface finishes; since we would only be able to scan one image, the best was to be chosen. Once selected, the sample was to be mounted onto a glass slide with a small piece of double sided tape. Mounted, the sample was loaded into the AFM, which was already prepared with an Olympus AC160TS probe (made from Si, it has a thickness of 4.6 µm while being 50µm wide and 160µm long a tetrahedral tip of 11 µm in length and a tip radius of <10 nm, a factory determined spring constant of 42 N/m, measured and calibrated to 45.94 N/m in the WPI AFM). [54]

[54] (Asylum Research, 2009)

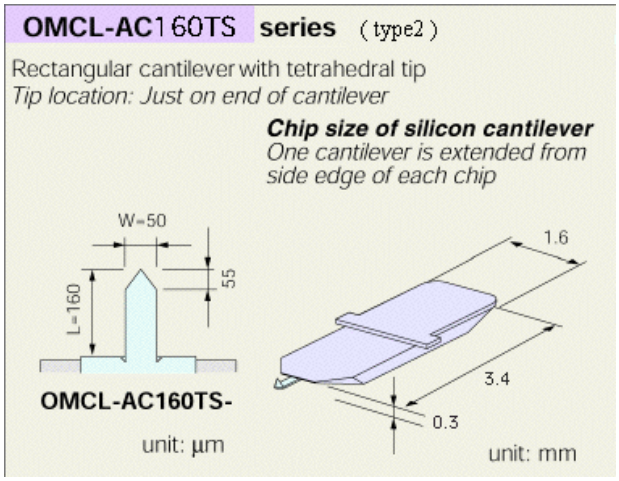

Figure 8: A manufacturer's diagram of the probe's geometry

As the sample was loaded, the cantilever was positioned over the sample and the laser, used for displacement measurement, was aligned accordingly. This was verified on-screen, as we could see the tip of the cantilever as well as the sample. From here, Sena loaded a pre-written parameter profile for the AFM, loaded in the proper spring constant and image size (20µm x 20µm), and started to scan the material. In order for the AFM to produce good results, we had to set the drive frequency (as the tapping mode requires the tip to oscillate at its resonance frequency, and find a suitable scan rate. The frequency was set to 321 kHz, and the scan took place at 4 Hz. While these settings were suitable, the controlling parameters needed to be fine-tuned in order to get clear, interpretable data. As the apparatus has a slew of controllers, the motion of the AFM probe is adjusted through a PID controller; once the AFM traces in one direction, it re-traces the same line, in order to get redundant data to check. If the magnitude of the constants for the proportional, integral or differential feedback equations are incorrect, it will manifest as the re-trace curve being mismatched to the original trace, and will result in a blurry, difficult-to-interpret image. Once the integral constant was tuned, each image was scanned, and resulted in two types of images; a height-based image and an amplitude-based image.

Height imaging is the most common way to collect the data. From the height images, section and roughness analysis can be done; these give quantitative results. As the tip moves across the surface, the probe is either retracted or extended (based on the topography of the surface) to maintain constant oscillation amplitude. The distance that the piezoelectric tube, which the sample sits upon, travels in the z direction is height; it is moved to maintain the oscillation amplitude. The data for height images are obtained based on this information, which are then analyzed and used to obtain physical data, such as roughness.

In amplitude imaging, the change in amplitude relative to the amplitude set point is collected. The topographical image (height image) gives the most quantitative data of the sample but it is low resolution compared to the amplitude image. Amplitude images are, in comparison, very high

resolution, where nanometer size structures can be seen easily. This mode of imaging is preferred to observe the fine details on the surface of the sample, but only as qualitative information.[55]

4.3.2 SEM Imaging

The observations of the morphology of samples were performed using a JSM-7000F (JEOL) scanning electron microscopy (SEM). There is no need for any special process to prepare the sample; just placing the samples into the SEM sample chamber, choosing the magnification, focusing the image, and then taking the pictures. The SEM found in the Mechanical Engineering department is to be be used on a scheduled basis by a trained and qualified operator.

4.3.3 Cyclic Voltammetry

The potentiostat was turned on. Each substrate was cut at 1x1 cm squares and placed in the electrochemical cell. The two parts of the cell were screwed together preventing the substrate from moving. 1 ml $K_3[Fe(CN)_6]$ solution was added on the substrate and the three electrodes were placed in their respective positions, staying soaked in the iron cyanide solution in contact with the substrate. The software available for the CV allowed the measurements of current vs. electric potential to occur. An electric potential span between -0.3V and 0.7V is measured. When the potential changes from 0.7V to -0.3V the surface is reduced and the peak occurs at around 0.18V. The oxidation graph shows a maximum while the reduction graph shows a minimum.

4.3.4 Surface Energy

Surface energy was measured using the goniometer. The sample was placed on an elevated stand with a camera facing the side of the surface. A small pump was used to transfer water from a beaker to a graduated dispenser which was programmed to hold the amount we specified in the computer software. The total amount we used was 500µl. The tube that passed through the pump sucked on one side water from a small beaker and placed it into the dispenser. The other side of the tube connected the dispenser to a 20µl pipette tip placed about 1 inch above the stand. In the software we specified the water ejection volume to be 2µl. Hence a 2µl water droplet would be slowly placed on the surface of interest. The camera would output the view into the computer which would in turn track the contrast between the background and the water droplet on the surface and by drawing tangents would measure two contact angles for each side of the drop and average them. About 6 drops, i.e. 6 measurements were obtained for each sample. Based on the contact angle results a qualitative conclusion can be obtained about the surface energy of each sample.

[55] (Ada, 2010)

5 Results and Discussion

The analysis of the different concentrations of magnetite nanoparticles based carbon substrates consisted of two different types of tests. In the cellular level it was determined whether the increase in nanoparticles concentration causes any change in nerve proliferation and differentiation. In the material characterization level the experiments tested for trends in surface energy, roughness, and electrical conductivity.

5.1 Cell Assay Tests

To quantify the differences between the samples in the cellular level a cellular adhesion assay was performed one day after the cells seeded onto the materials.

5.1.1 Cell Adhesion Test

The total number of cells was determined for the five types of substrates and the results are plotted in Figure 9, as shown.

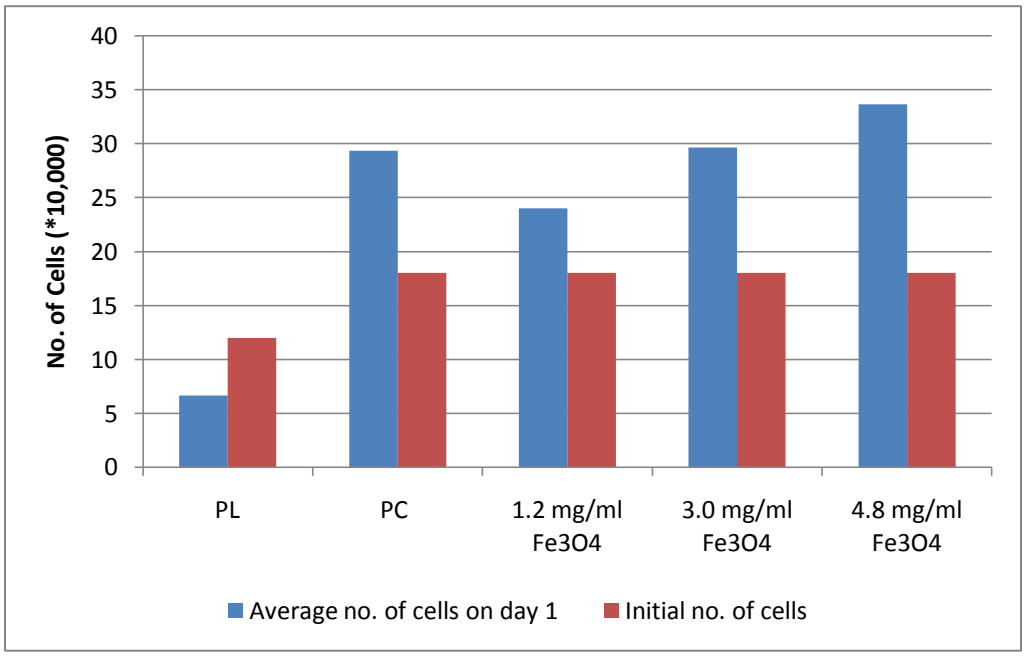

Figure 9: Average number of cells adhered on day 1 compared to the seeding number of cells on day 0 (PL stands for the poly-D-lysine coated cover slips, PC stands for plain carbon)

The seeding concentration as explained in the methodology was $5*10^4$ cells/cm2. This number was converted to a total number of cells based on a 1 ml volume. Since the poly-D-lysine coated cover slips had a smaller surface area, the seeding number of cells was $12*10^4$ as opposed to $18*10^4$ cells for the carbon based substrates. Two observations can be made based on the graph. When compared to poly-D-lysine coated cover slips, PC-12 cells have a noticeably greater affinity for the carbon-based substrates. The lower average number of cells on day 1 for poly-D-lysine is due to the fact that one day is not enough for all the cells to adhere. Therefore some cells were aspirated out before treatment with trypsin, and hence before the cell counting process. The second observation regards the comparison of

all the three magnetite doped carbon substrates. As it can be seen from the graph, there is a trend of increased cell proliferation as the concentration of magnetite nanoparticles increases. The plain carbon coated substrates, unpredictably, have a greater cell proliferation effect compared to the 1.2 mg/ml magnetite based wafer. PC-12 cells have at least 4 times greater affinity than the carbon based substrates. The magnetite doped substrate at a concentration of 4.8 mg/ml nanoparticle solution shows about 15% greater affinity than plain carbon in terms of cell growth.

5.1.2 PC-12 Culture on Substrates (no NGF added)

In addition to their proliferation affinity, the samples were also tested for their ability to promote differentiation. About 200 cells per type were chosen randomly and the average neurite length was measured. The results are shown in Figure 10.

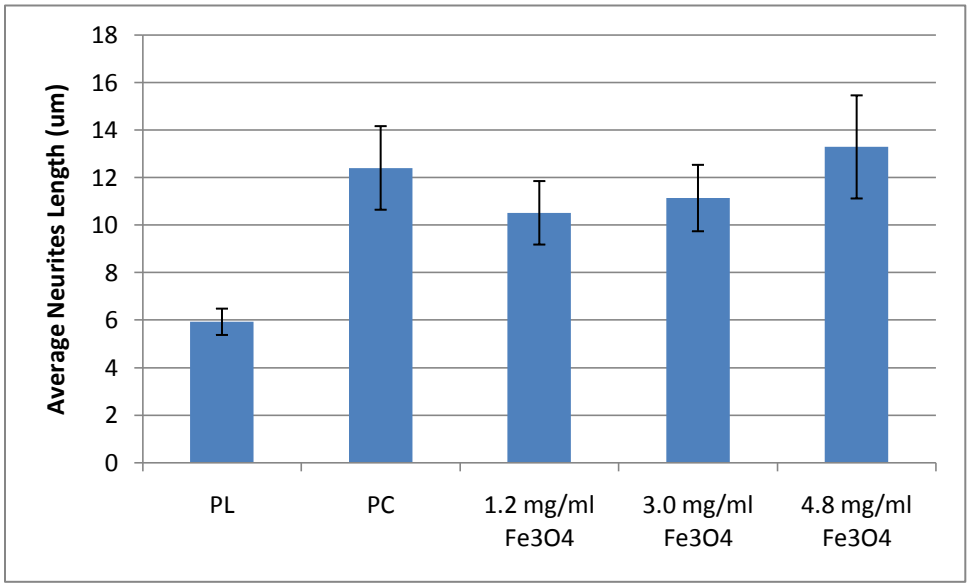

Figure 10: The average length of neurites for all the different substrates (no NGF added). PL refers to poly-D-lysine. PC refers to plain carbon.

Based on the graph it can be concluded that the carbon based substrates represent a significant improvement compared to the common poly-D-lysine cell culture experiments in terms of neuronal differentiation. There also seems to be a direct relationship between the concentrations of magnetite nanoparticles to neurite length. Larger concentrations of nanoparticle solutions demonstrate particular interest for further experimentation. Figure 10 gives a representation of the cells attached to each of the substrates. The results about the neurite length can be certainly noticed in the representative picture. The neurite length is larger for the carbon substrate with 4.8 mg/ml magnetite concentration solution.

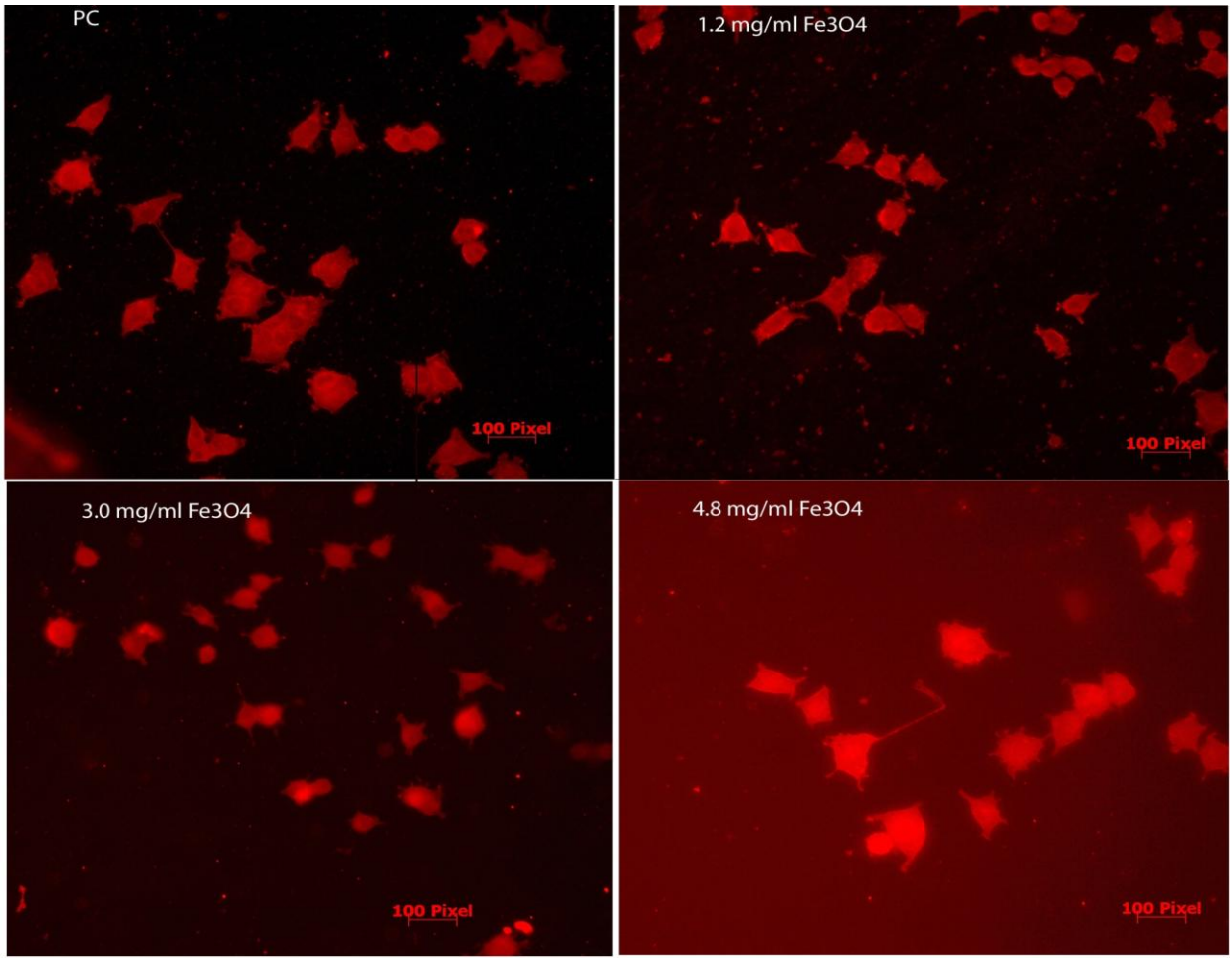

Figure 11: Neurite length pics selected for each of the different substrate concentrations.

5.1.3 PC-12 Culture on Substrates (NGF added)

The analysis of neurite length for the NGF cultured PC-12 cells was particularly challenging because, due to their reaction with NGF, most neurites were quite long and often intertwined with the neurites of neighboring cells. Hence it was difficult to tell the difference. There was also a great variety of lengths, starting from the very small ones to the extremely large ones. Averaging all the numbers generated the results in Figure 14.

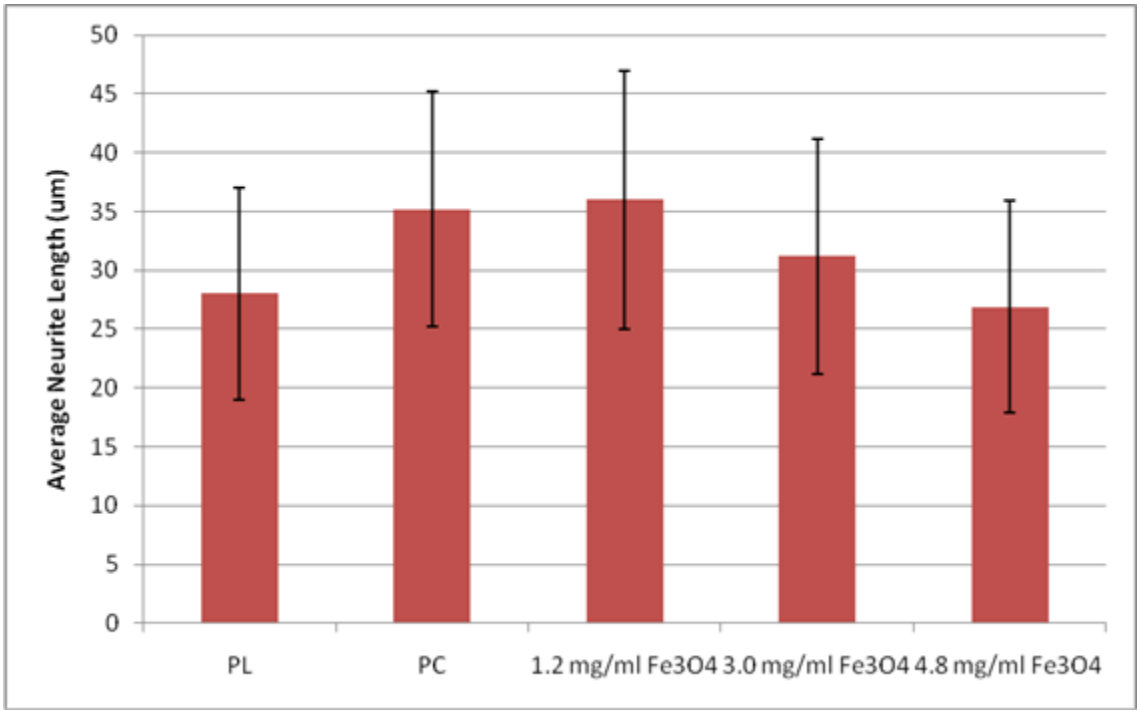

Figure 12: The average length of neurites for all the different substrates during the differentiated case (NGF added). PL refers to poly-D-lysine. PC refers to plain carbon.

Although on average it seems that the sample at 1.2 mg/ml magnetite solution concentration generated the longest length, we are hardly able to draw any strong conclusions regarding the difference in cell behavior due to the large inaccuracy, particularly because of the challenge previously mentioned. Our main conclusion in this case is that NGF sees no difference when reacting with the carbon-based samples as opposed to the poly-D-lysine cover slip. Hence, our sample does not interfere with NGF's activity.

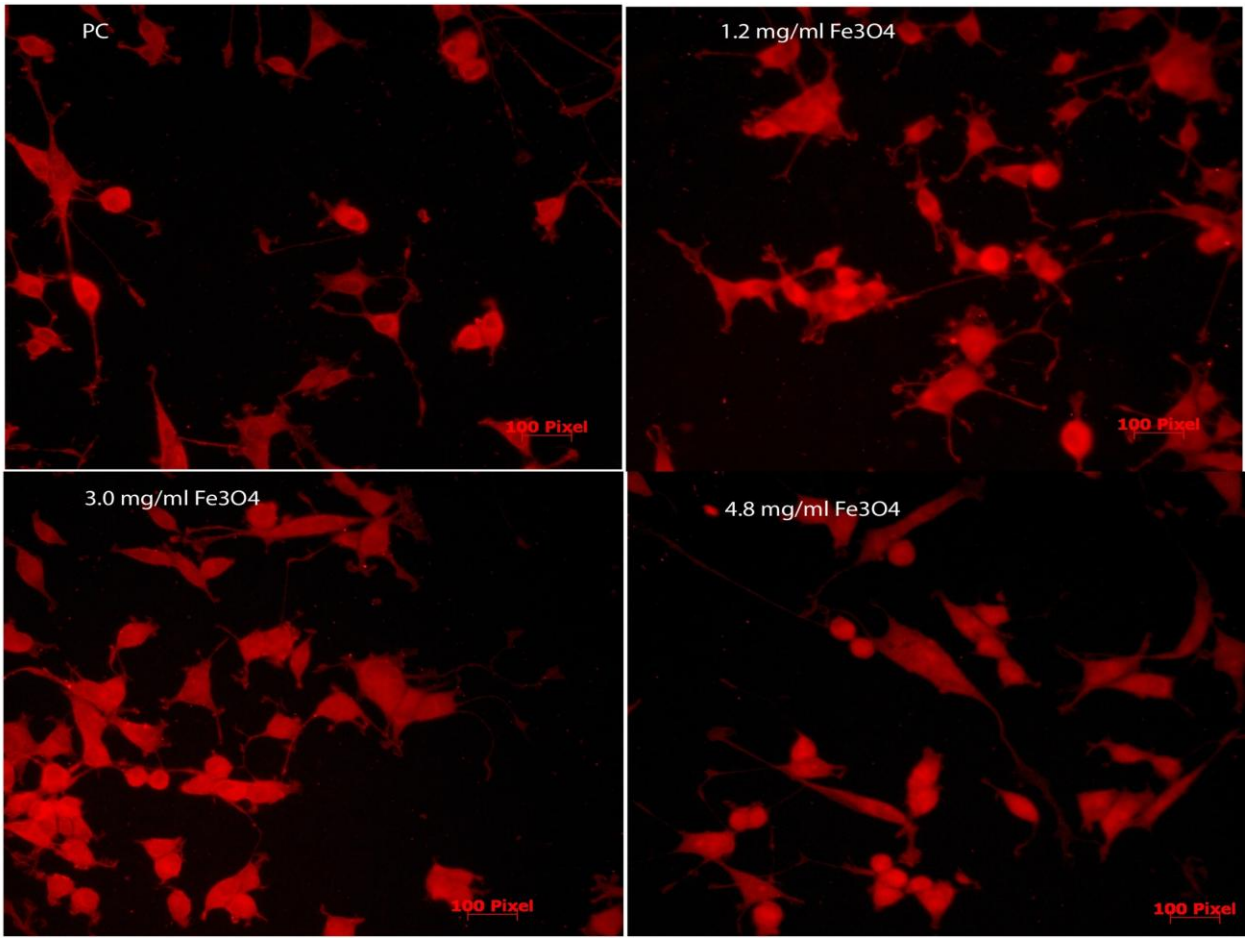

Figure 13: Neurite length pictures selected for each of the different substrate concentrations

5.2 Material Characterization

The characterization of the material is highly important because it might give insight into the effects of the physical and chemical properties on cells and their life cycle. For our project we aimed at surface energy, roughness, and electrical conductivity. To test these characteristics, three equipment were used respectively, the goniometer, the atomic force microscope, and the cyclic voltammeter.

5.2.1 Surface Energy

The contact angle was tested with water considering that human cells float in a sea of water and the growth media used are water based. A lower surface energy corresponds to a more round droplet because the water-air energy dominates as opposed to the water-surface energy. A more round droplet is characterized by a larger contact angle. The results of the experiment are shown in Figure 14.

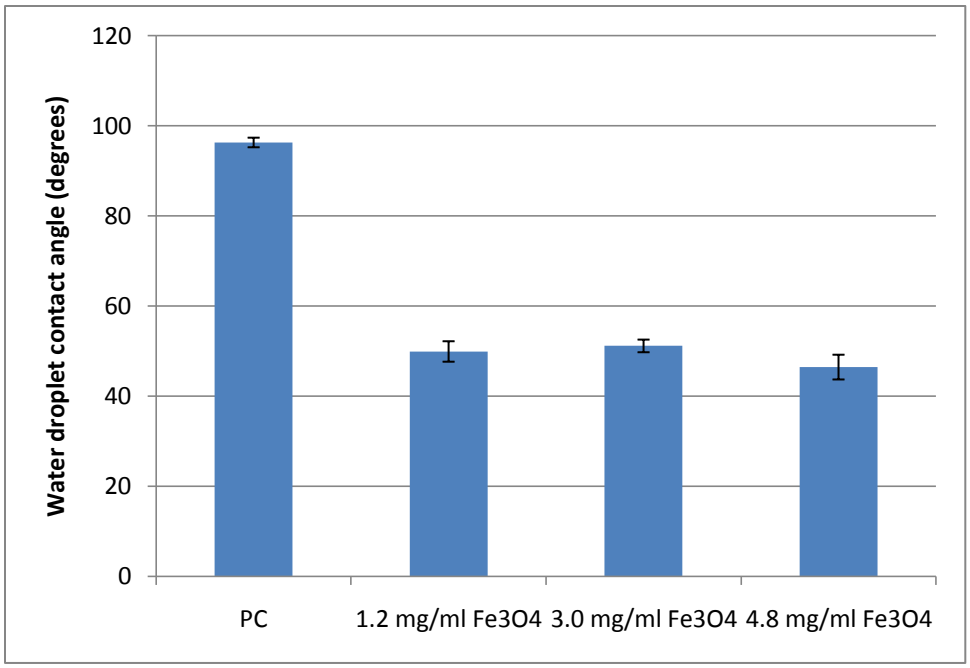

Figure 14: The contact angle between a water droplet and the respective carbon substrate (PC represents plain carbon)

Although no difference is noticed between the three concentrations of iron oxide in the contact angle, it is evident that the contact angle for the plain carbon surface compared to the nanoparticle-based surfaces is greater. In terms of surface energy, the iron oxide-nanoparticle substrates contain more surface energy than the plain carbon. There is a subtle decrease in 4.8 mg/ml Fe3O4 compared to 1.2 and 3.0 mg/ml which could be more noticeable at higher concentrations. However, comparing to the results from the cell culture assays, there is no obvious relationship between surface energy and cell growth/differentiation.

5.2.2 Roughness

The roughness of the surface was determined using the atomic force microscope located in the ground floor of Gateway Park. Figure 15 shows the elevation as a function of position x and y for all four carbon surfaces.

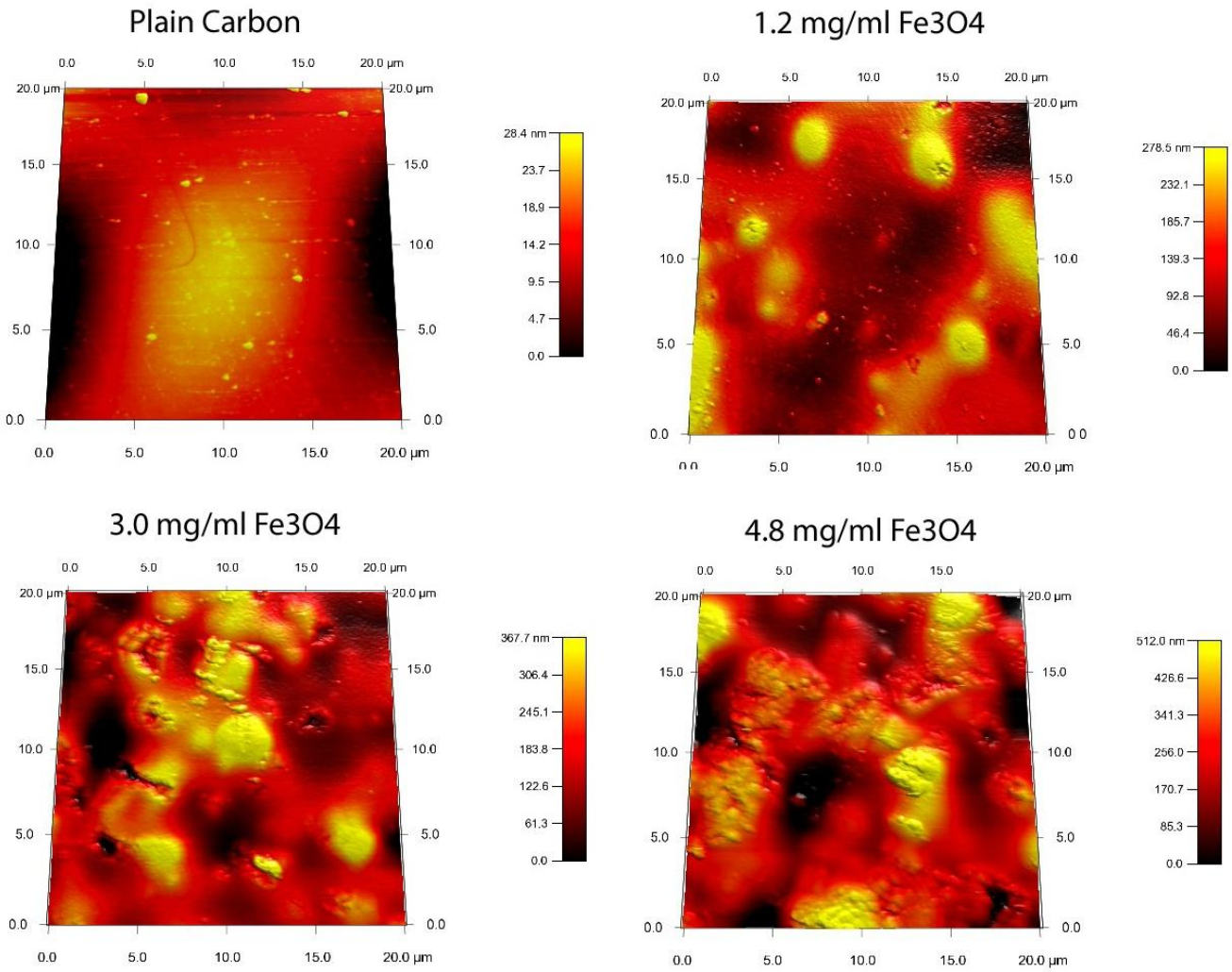

Figure 15: AFM pictures for all the carbon substrates

The area set for analysis was 20µm x 20µm. The program that operated the AFM generated the root

mean squared values (RMS) which determined the roughness of each sample. The results are plotted graphically in Figure 16 as a better means of comparison.

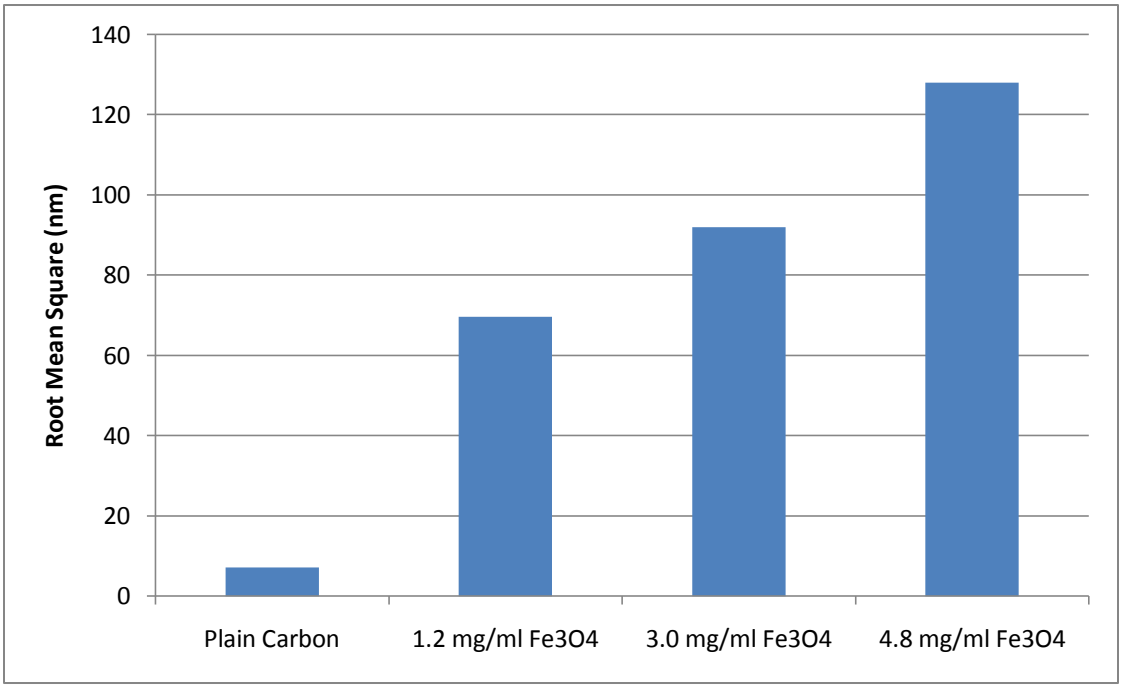

Figure 16: RMS values of the surface elevation for all carbon-based substrates obtained using the AFM. The RMS value represents the roughness of the material.

The increase in concentration shows an obvious increase in surface roughness. In terms of results, we can clearly see a trend between the adhesion of the cells and the roughness of the surface. While this has been proven in previous experimentation, the next step would be to try larger, more widespread variation of nanoparticles concentration in order to see how the relationship works: if we are able to find an empirical equation (i.e, the number of cells that adhere and the roughness are related linearly until a certain point, as other sources suggest), we can find this optimal roughness, calculate what concentration of nanoparticles could achive this, and fabricate using this number. From here, we can see what, exactly, the neurons do.

5.2.3 Cyclic Voltammetry

The property of electrical conductivity can be analyzed using the current vs. electric potential graphs. The higher peaks are an indication of the higher conductivity of a material. Based on this factor, after looking at the results in Figure 17, greater concentrations of magnetite allow for greater surface conductivity.

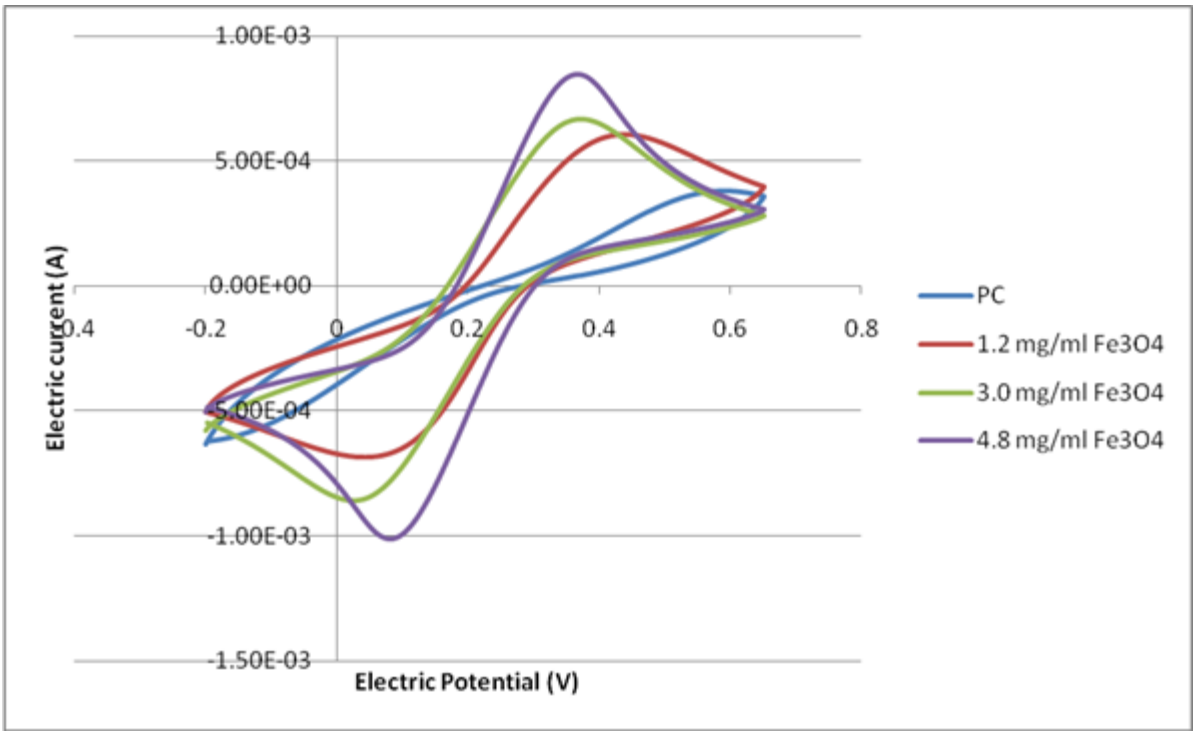

Figure 17: CV results for the four different carbon based substrates

The first observation that can be made from figure 16 is that all carbon samples are conductive. A non conductive material would show a straight horizontal line with 0 ordinate. The plain carbon sample generated an unusual shape as it has been extracted in figure 17. Hardly any peak is observed, they are not at the optimal potentials of 0.18 and 0.22 V.

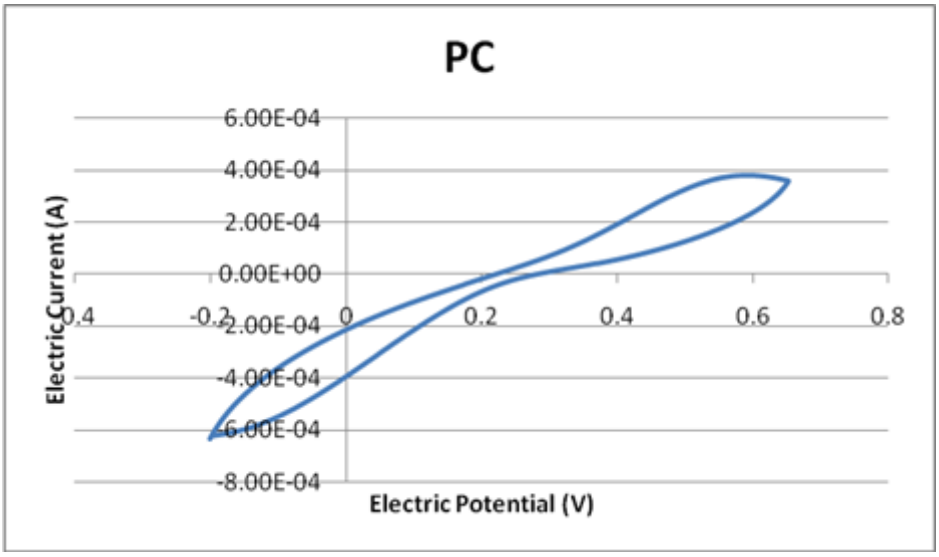

Figure 18: CV results for plain carbon alone

The 1.2 mg/ml magnetite concentration sample generated two peaks, one at 0.07 V and the other at 0.43 V. The material is conductive but since the peaks are not as sharp compared to the other results, it is not greatly conductive. The result is extracted in figure 18.

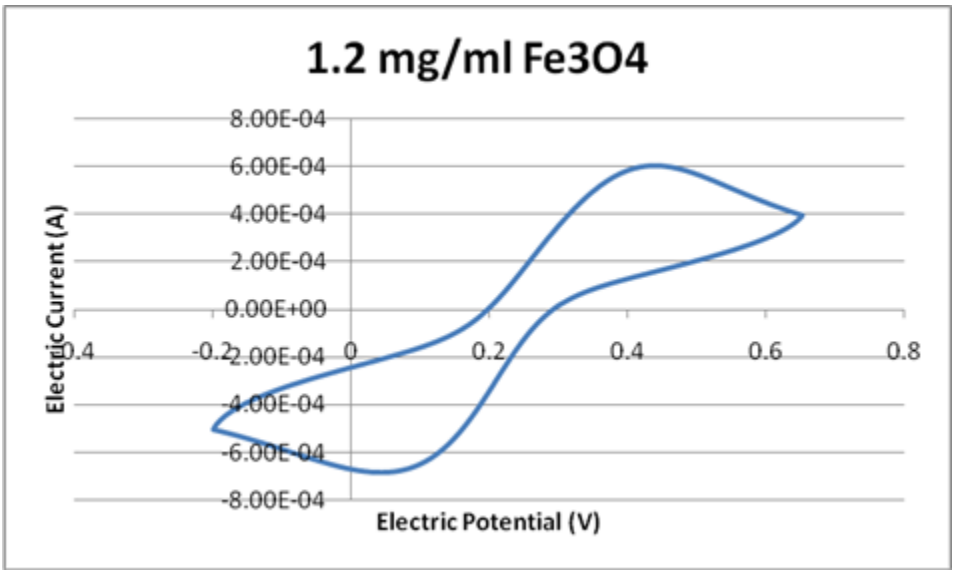

Figure 19: Results for the 1.2 mg/ml magnetite sample only

The 3.0 mg/ml magnetite concentration sample generated two obvious peaks, one at 0.03 V and the other at 0.37 V. Compared to 1.2 mg/ml and plain carbon, the peaks are much closer to the desired potential peaks of 0.18 V and 0.22 V. As it is shown in figure 19, they are also much sharper and at a greater current span.

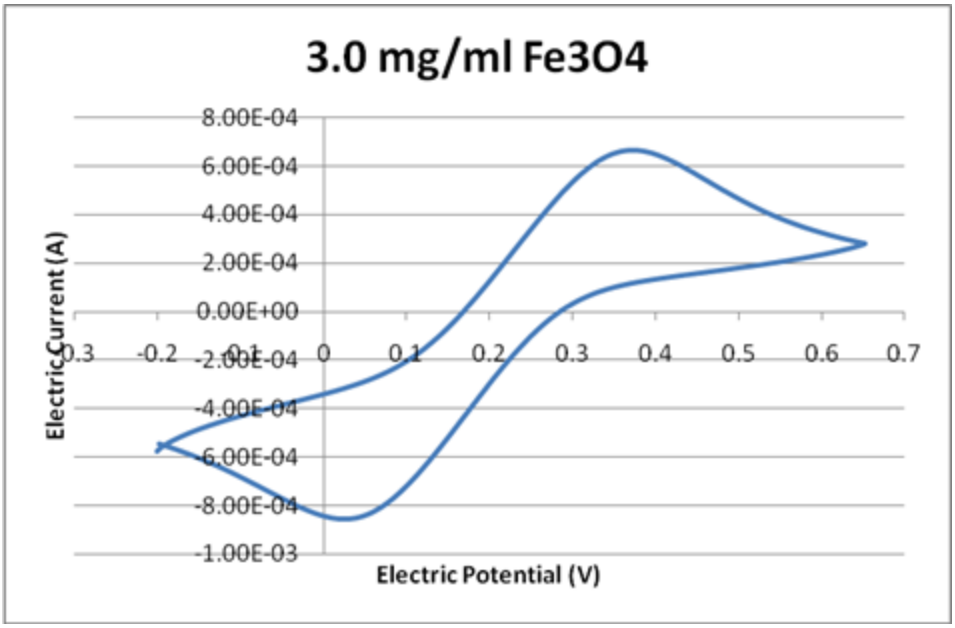

Figure 20: CV Results for the 3.0 mg/ml magnetite sample only

The 4.8 mg/ml magnetite sample generated two peaks, one at 0.11 V and the other at 0.35 V as shown in Figure 20. This sample generated the best results in terms of sharpness or current span and the reduction and oxidation peaks are much closer together than the previous three samples.

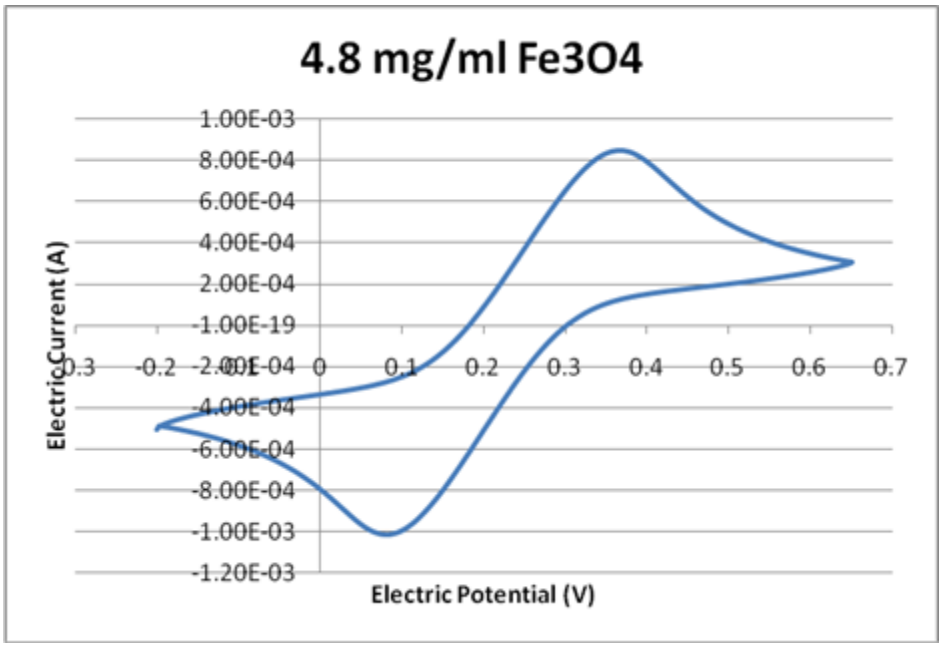

Figure 21: CV Results for 4.8 mg/ml magnetite sample only

5.2.4 SEM Imaging

SEM Imaging provides a qualitative rather than quantitative analysis of the material properties. This analysis is in itself very accurate due to the microscope's large precision. We are able to get a good idea of the physio-chemical properties of the material through the other tests that are run; however, much of the neuron-material interaction is physical, and having the proper images can lead us to understanding the particulars of the physical contact made between the two species. From the previous testing, we understand that the cells tend to propagate and adhere better to the Fe_3O_4 samples; we also know that the surface gets rougher as the concentration of magnetite increases. With this in mind, the samples are imaged, the results in Figure 22.

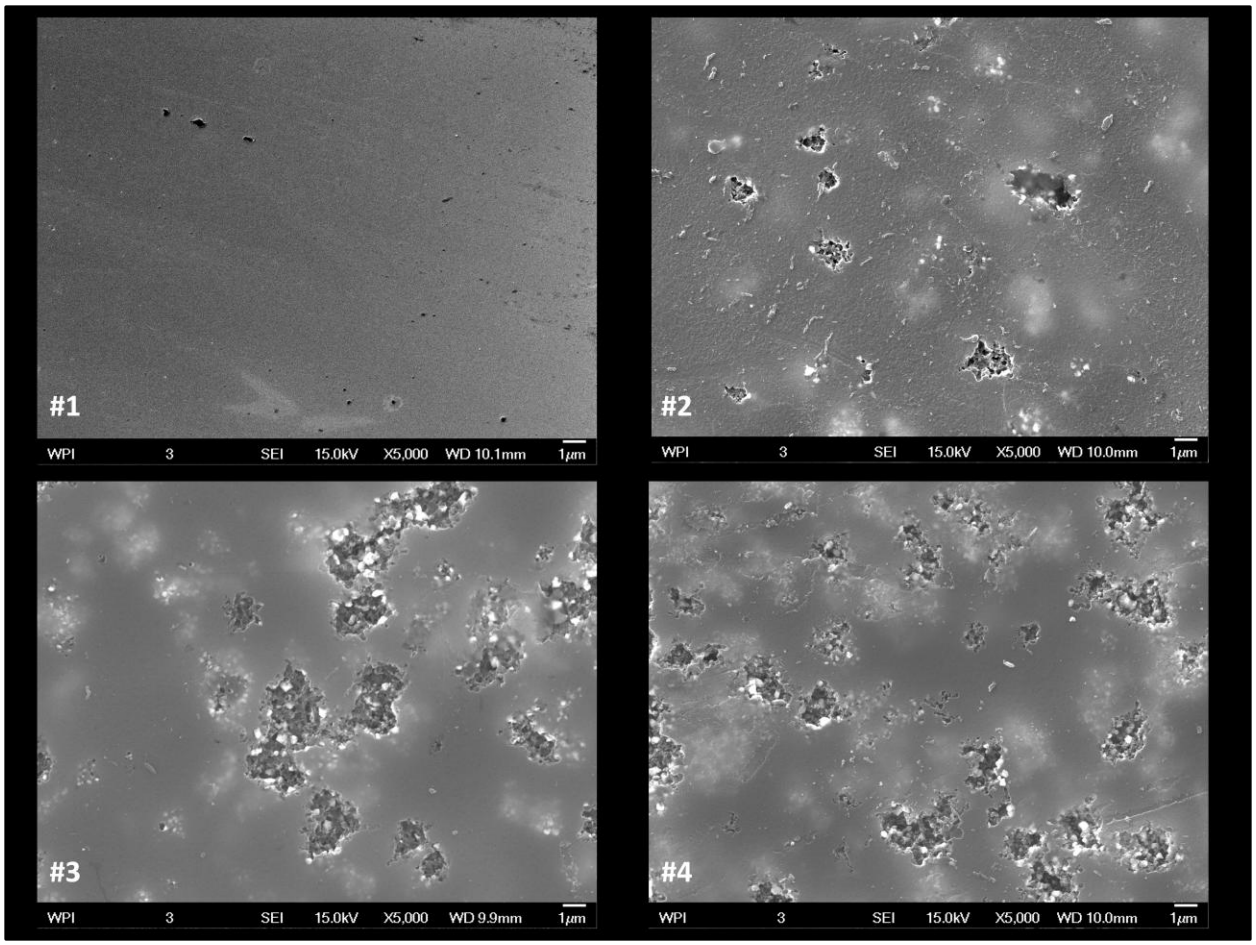

Figure 22: SEM pictures for plain carbon (top left), 1.2 mg/ml magnetite (top right), 3.0 mg/ml magnetite (bottom left), 4.8 mg/ml magnetite (bottom right)

The images obtained clearly show an increase in surface phenomena with an increase in concentration of magnetite. While this has already been discovered with the amplitude images found during the AFM analysis, it is the level of detail that we get with the SEM that sheds light on what these phenomena are. The first step is to differentiate between the plain carbon samples from the magnetite doped one, in terms of surface phenomena. From the images, we see lighter spots, seeming made up of small dots, on numbers two, three and four. Additionally, we have the darker, corrosion-like spots, and their density increases with the concentration of magnetite. These two phenomena are seen on the magnetite doped samples, exclusively.

First, the lighter particles seem to be either on the surface (as seen on the bottom right corner of the #2 sample; the outline of the white can be more clearly seen) or underneath the surface (as seen in the top left corner of sample #3). This alludes to the phenomena being particulate, which gives the sense that these are clumps of nanoparticles that are on or underneath the surface. However, these could also be something entirely different; this explanation uses the darker phenomena, which requires a closer view.

Using a close-up view at 25,000X magnification of the corrosion-like phenomena, shown in Figure 23, we can see bits of the lighter phenomena in the upper right hand corner.

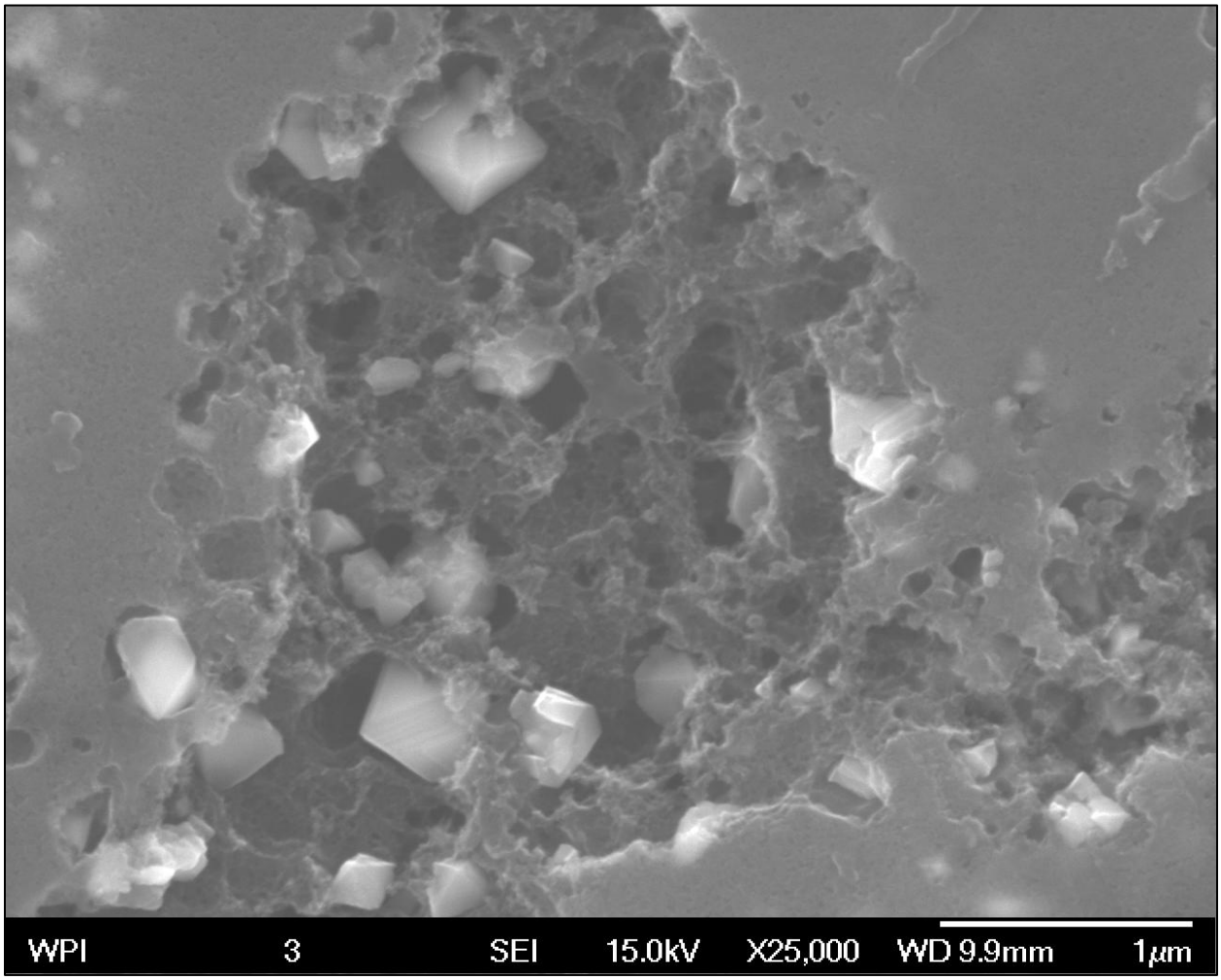

Figure 23: 25,000X magnification of one of the surfaces showing the corrosion-like phenomenon

In terms of the darker phenomena, it is difficult to tell weather this is a depression into the material or, rather, something that is raised off of the surface. From the AFM roughness data, we were lead to believe that these were extruded from the surface. One explanation can explain both; the darker appearance (a recession in the material) and the extruded phenomena (out of the surface).

Take the lighter phenomena we had seen; we have claimed it is slightly underneath the surface. Consider that the lighter spots are bubble; thee surface appears lighter as there is something underneath or the surface has been deformed outwardly due to some internal pressure. The darker phenomena look like recessions, almost etched or corroded away. It is possible that the darker spots are where a bubble had formed and, instead of staying underneath the surface, it had popped. Because the surface had been stretched out, it appears to be higher than the rest of the surface, whereas the inside is slightly lower than the rest of the surface. The idea that the dark phenomena is the inner part of the

surface in interesting, especially given the web of material that we see. The origin of the bubble is unknown, but consider the process of pyrolysis: we are taking carbon, doped with magnetite, and heating it to 1000°C. The magnetite has a higher heat capacity than the carbon, and will ultimately be hot longer. If the nanoparticles retain heat after the carbon cools, perhaps some epoxy around this hot mass of nanoparticles is still burning off, but trapped underneath the surface. Thus, while cooling, bubble form underneath the surface. The more nanoparticles, the more sites for this, therefore the more phenomena. If the pressure is too high in the bubble, they burst. This explanation does correlate with what we see with the SEM data.

The internal surface does not look like that of the surface for plain carbon, as it is flat and plain, but is rather twisted. We believe that these are the genesis of carbon nanotubes. Nanotubes are commonly formed by the activation of carbon over precious metals, alloys, and even iron oxides. The particles act as a catalyst for their formation. A picture of these nanotubes, taken from a UCLA report, shows the nanotubes formation.

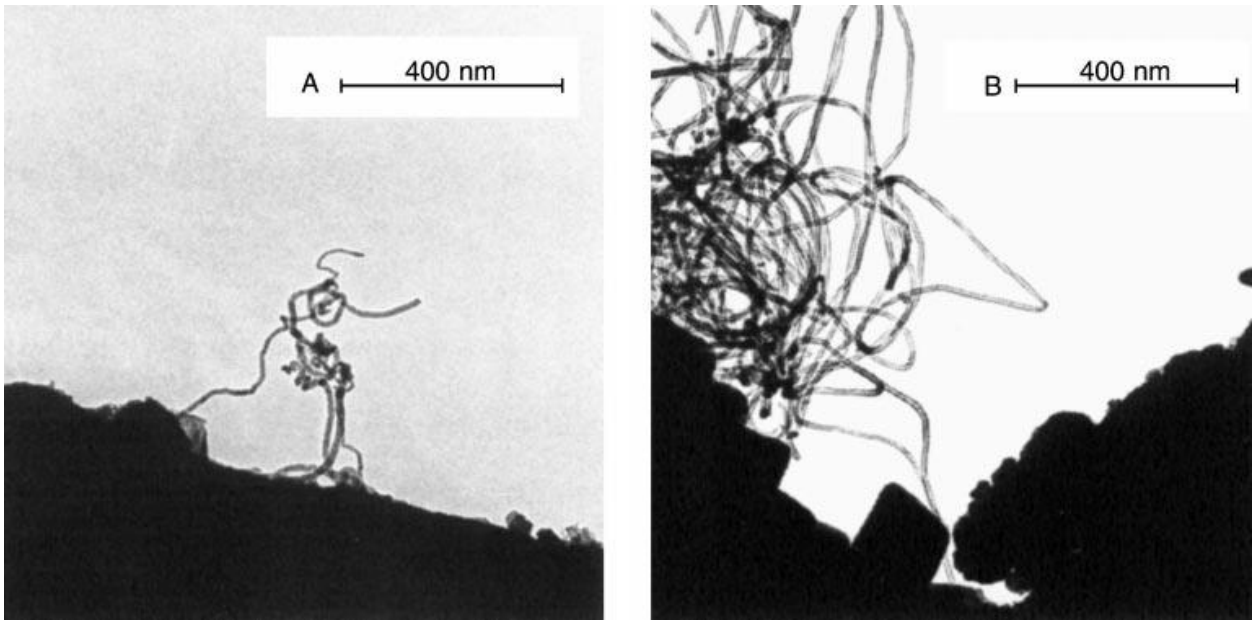

Figure 24: Carbon nanotubes fabricated over a precious metal catalyst.

While this cannot be determined by analytical tools we had available during the scope ofthis project, it would be interesting to test and see nanotubes could be produced in such a fashion, or if we are simply seeing the inner carbon being less compacted and still retaining a folded, epoxy shape. Either way, the exact surface phenomenon is unknown, but does open up interesting possibilities that can, and should, be further analyzed.

6 Conclusions and Recommendations

The experimentation done over the duration of this project has yielded significant data, enabling us to conclude that our engineered material promotes the proliferation of PC-12 cells, as well as showing physical and chemical properties that correlate with the concentration of the magnetite nanoparticles. The results of the material testing that the substrates underwent largely correlated with the amount of nanoparticles that we had doped the surface with.

The cyclic voltammetry testing is a good and clear indication of the electrical conductivity of the material. The higher and closer to the origin the peaks occur at, the more conductive the surface is. There is a clear trend, with the resulting shape, that indicates the superior conductivity of the magnetite-doped surface; while an insulating material would show a completely flat line, the plain carbon, the least conductive of the materials, is the closest to being flat, with the peaks of the doped materials becoming larger as concentration increased. This is strong, supporting evidence that the concentration of the MNPs are accurate, as the electricity is able to flow between the magnetite, a better conductor then the carbon, thus reducing the resistance given by the material. This shows that, even after pyrolysis, the magnetite is present in the material in concentrations reflective of the amount seeded during spin coating. This shows that either the magnetite is lost at a constant rate during pyrolysis, or that the magnetite is retained as the epoxy is pyrolyzed, with little to none being lost. Either way, this observation validates the pyrolysis procedure as a repeatable, controlled step in our fabrication process.

The surface energy measurements offer both a quantitative and qualitative representation of the surfaces in terms of their respective energies. The lower contact angle for all of the doped samples leads us to believe that, while the surface energy is increased by the presence of the nanoparticles, the concentrations that we tested were either too closely spaced to show a significant difference, or we are approaching the asymptote at which the surface energy can be increased by magnetite as a surface additive.

The RMS roughness analysis showed a clear increase in the surface roughness of the substrates with an increased concentration of magnetic nanoparticles. While the AFM images did show an increase in the number of surface phenomena, it was the height of the differences that weighed most heavily on the roughness analysis. The increased number of nanoparticles on a surface leads to and increased height that the surface phenomena achieve; as the surface phenomena seems to be created as a result of carbon being activated over the MNPs during pyrolysis, the higher concentrations not only increase the number, but also the magnitude, heavily suggesting the dependence of the phenomena on the MNPs.

The SEM images, while being qualitative, show a definite increase in the surface phenomena. Coupled with the AFM images, we can project that the height of these phenomena are also larger. Research has been done dealing with the catalysis of carbon nanotubes over precious metals, as well as other metallic compounds, one of which being iron oxide, including magnetite. While not the best catalyst, it is still able to produce nanotubes. While the sub-structure inside the phenomena is unknown, they do appear to be carbon, constructed in a web-like fashion which could be a precursor to these nanotubes.

However, more detailed SEM images, as well as isolation and characterization of these structures must be carried out to confirm exactly what this substructure is, and its composition, with any certainty.

The neuronal cell testing done has led for us to conclude that the amount of MNPs affects the rate of cell proliferation. The cell adhesion test and non-NGF trials show that the doped surfaces perform better than the laboratory-standard poly-D-lysine coated glass. While the protein has been formulated for cell adhesion, the properties of our substrate appear to be beneficial to cell adhesion and proliferation. However, the advantages of this material seem to be negated once the system is introduced to NGF; once added, the cells show no difference between the doped and non-doped surfaces.

While the scope of this project has been large, the next steps that can be taken would further validate the data found within this project, but also explore the potential of this substrate as a true base for neuron culture. First, the concentrations of the magnetite nanoparticles should be used on a larger scale to see the long-range, edge-of-the-envelope scenarios, and the implications on the physical and chemical properties. Testing small amounts could lead to a threshold value of how many MNPs need to be added before changes in roughness, electrical conductivity and surface energy can be seen, and, on the other side of the spectrum, how many MNPs are needed to reach the limit of our measurable parameters. As we have identified these variables, such as roughness, as important factors, we advise the testing of other materials, such as plastics or mineral-doped zeolytes, for cell culture, to see if a material characteristic is constant over a wide range of materials; from these observations, the carbon surface can be tuned to the most beneficial found value through the fabrication process. Once an ideal material has been found and can be created, taking advantage of the UV-active property of the epoxy and using photolithography to create a pattern could potentially lead to neuronal guidance, having the neurons grow into a pre-planned network that could ultimately be utilized for a biomedical application.

In terms of cells, additional types of neuron cells should be tested. While PC-12 cells are a good reflection of a human neuron may do, we must look to see if other cells will act the same way. The first step would be the utilization of dorsal root ganglia (DRG) cells. Being part of the peripheral nervous system, they are primary neurons that transmit information directly from the CNS, usually the spinal cord. DRG cells are found in all mammals, however, in the lab at UMass Medical School, they are extracted through the dissection of a chick's embryo. The next steps up in terms of complexity are stem cells, commonly those coming from the bone marrow. These undifferentiated human cells can be instructed to differentiate into CNS neurons as long as the necessary growth factors are provided. This material, based on the ability to guide cells, could prove the key to creating a controlled network of human nerve cells that could be used for nervous system repair, as well as a staging area for the cells to grow while in the body.

One of the most exciting current research topics consists in discovering the mechanism, the pathway that a neurite follows when extending and what changes when it then differentiates into an axon with no further growing capabilities. Such a discovery would lead to novel approaches to neuroregenerative medicine. This is one of the main factors behind the motivation for the design of the available substrate for nerve cell growth.

7 Works Cited

A. Ahmed, C. B. (2002). Bioadhesive microdevices with multiple reservoirs: A New platform for oral drug delivery",. *J. Controlled Release* , 291-306.

A. Desai, W. C. (1997). Microfabricated biocapsules for cell xenografts: A Review. *Proc. SPIE, Micro and Nanofabricated Electro-Optical-Mechanical Systems for Biomedical and Environmental Application* , 216-226.

A. M. Lyons, L. P. (1985). Photodefinable carbon films: Control of image quality. *J. Vac. Sci. Technol. , 3* (1), 447-452.

Ada, S. (2010, 3 20). Introduction to AFM. (O. R. M.Perrone, Interviewer)

Akira Ito, M. S. (2005). Medical application of functionalized magnetic nanoparticles. *Journal of Bioscience and Bioengineering , 100* (1), 1-11.

Asylum Research. (2009). *Asylum Research AFM Cantilvers*. Retrieved 2010, from http://www.asylumresearch.com/Products/Levers/AC160.shtml

Baselt, D. (1993). *The tip-sample interaction in atomic force microscopy and its implications for biological applications.* California Institute of Technology.

Boston, C. H. (2007). *The neuron*. Retrieved from http://www.childrenshospital.org/research/_neuron/index.html

Bruno Wacogne, C. P. (2008). Measuring the mechanical behaviour of human oocytes. *Biomed Microdevices , 10*, 411-419.

Bunge, R. a. (1983). Interrelationship between Schwann cell function and extracellular matrix production. *Trends in Neuroscience , 6*, 499-505.

C.C. Berry, S. W. (2004). Cell response to dextran-derivatised iron oxide nanoparticles post internalisation. *Biomaterials , 25* (23), 5405–5413.

Chang A., S. M. (2009). BRENDA, AMENDA and FRENDA, The Comprehensive Enzyme Information System: EC 3.4.21.4 - trypsin. *Nucleic Acids Res. , 37*, Database Issue, D588-D592.

Chollet, F. (2009, 2 15). *A (not so) short introduction to MEMS.* Retrieved 2 15, 210, from MEMScyclopedia.org: http://memscyclopedia.org/Document/introMEMS.pdf

Cornell, R. M. (1996). *The iron oxides : structure, properties, reactions, occurrence and uses.* Weinheim, Germany: VCH.

D. Vaudry, P. S. (2002, May 31). Signaling Pathways for PC12 Differentiation: Making the Right Connections. *Science, AAAS* , pp. 1648-1649.

Dr. Olivier J. A. Schueller, D. S. (1996). Fabrication of glassy carbon microstructures by pyrolysis of microfabricated polymeric precursors. *Advanced Materials , 9* (6), 477-480.

Feitknecht, W. &. (1970). Mechanisms for the Oxidation of Fe3O4. *Nature* , 548 - 549.

Foundation, W. E. (2001). *The Human Brain*. Retrieved from Discovering Psychology: http://www.learner.org/discoveringpsychology/brain/index.html

Gallagher, K. J. (1968). Mechanism of Oxidation of Magnetite to [gamma]-Fe2O3. *Nature* , 1118 - 1121.

Goldstein, J. (1992). *Scanning electron microscopy and X-ray microanalysis : a text for biologists, material scientists, and geologists* . New York: Plenum Press.

Grayson, A. S. (2004). A BioMEMS review: MEMS technology for physiologically integrated devices. *Proceedings of IEEE*, (pp. 6-21).

Hafeli, U. P. (April 1999). In vitro and in vivo toxicity of magnetic microspheres. *Journal of Magnetism and Magnetic Materials , Volume 194* (1), 76-82.

Howard, K. (1999, April 5). *Do Brain Cells Regenerate?* Retrieved from Princeton Weekly Bulletin: http://www.princeton.edu/pr/pwb/99/0405/brain.htm

Hui Hu, Y. N. (2004). Chemically Functionalized Carbon Nanotubes as Substrates for Neuronal Growth. *Nano Letters , 4* (3), 507–511.

Inc., K. S. (2009). *Hank's Balanced Salt Solution (HBSS)*. Retrieved from Krackeler Scientific Inc.: http://www.krackeler.com/products/1451-Balanced-Salt-Solutions/14473-Hanks-Balanced-Salt-Solution-HBSS-.htm

Indiana State University. (2007, 5). *How SEM Works*. Retrieved 3 6, 2010, from http://mse.iastate.edu/microscopy/path2.html

Invitrogen. (2009). *DMEM - Dulbecco Modified Eagle Medium*. Retrieved from Invitrogen Corporation: http://www.invitrogen.com/site/us/en/home/Products-and-Services/Applications/Cell-Culture/Mammalian-Cell-Culture/Classical_Media/dmem.html

Invitrogen. (2002). *LipofectamineTM 2000.* Retrieved from Datasheet catalog: http://www.datasheetcatalog.org/datasheets2/14/145541_1.pdf

Ito, A. H. (2004). Construction and harvest of multilayered keratinocyte sheets using magnetite nanoparticles and magnetic force. *Tissue Engineering , Vol. 10*, 873-880.

James V. Crivello, T. C. (1997). Fabrication of Epoxy Matrix Composites by Electron. *Chem. Mater* , 1273-1284.

Jean Hopkins, C. W. (2003). *Human Biology and Health.* New Jersey, USA: Englewood Cliffs.

Jian Ying Zhanga, E. J. (June 2000). A new peptide-based urethane polymer: synthesis, biodegradation, and potential to support cell growth in vitro. *BioMaterials* , 1247-1258 .

Johnson, E. J. (1988). Expression and possible function of nerve growth factor receptors on Schwann cells. *Trends in Neuroscience , 11*, 299-304.

Kircher MF, A. J. (2002). Intracellular magnetic labeling with CLIO-Tat for efficient in vivo tracking of cytotoxic T cells by MR imaging. *Radiology* , 453.

L.X. Tiefenauer, A. T. (1996). In-vivo evaluation of magnetite nanoparticles for use as a tumor contrast agent in MRI. *Magnetic Resonance Imaging , 14* (4), pp. 391-402.

Ling Zhang, R. H.-C. (2006, December 30). Oleic acid coating on the monodisperse magnetite nanoparticles. *Applied Surface Science* , pp. 2611-2617.

Lloyd A. Greene, A. S. (1976). Establishment of a noradrenergic clonal line of rat adrenal pheochromocytoma cells which respond to nerve growth factor. *Proc. Natl. Acad. Sci.* , 2424-2428.

Mattson, M. P. (Dec 30, 2003). *Patent No. 6670179.* US.

Ming Zhao, S. M. (2003). Evidence for neurogenesis in the adult mammalian substantia nigra. *Proceedings of the National Academy of Sciences* (pp. 7925-7930). The National Academy of Sciences.

Nerve Regeneration. (n.d.). Retrieved from http://biomed.brown.edu/Courses/BI108/BI108_2001_Groups/Nerve_Regeneration/

Nonaka, K. (. (1998). *Patent No. 5834661.* Japan.

Olle Lindvall, R. M. (2003). Brain repair by cell replacement and regeneration. *Proceedings of the National Academy of Sciences* (pp. 7430-7431). The National Academy of Sciences.

P. Moroz, S. J. (2002). Magnetically mediated hyperthermia: current status and future directions. *Int J Hyperther , 18* (4), 267-284.

Paik, M.-J. Y.-W. (2002). The Contact Resistance and Reliability of. *IEEE TRANSACTIONS ON ADVANCED PACKAGING* .

Pampuro, R. (2009). *Photoresist Derived Carbon as a Substratum for Nerve Cell Culture.* Worcester, MA: WPI.

Pisanic, T. R. (2007). Nanotoxicity of iron oxide nanoparticle internalization in growing neurons. *Biomaterials , 28*, 2572–2581.

Pohanka, M., Jun, D., & Kuca, K. (2007). Mycotoxin Assays Using Biosensor Technology: A Review. *Drug and Chemical Toxicology , 30* (3), 253-261.

R. Weissleder, D. S. (1989). Superparamagnetic iron oxide: pharmacokinetics and toxicity. *American Journal of Roentgenology , 152*, 167.

R.J.M. Franklin, W. B. (1990). The peripheral nervous system-central nervous system regeneration: a role for glial cell transplantation. *Journal of Cell Science* , 185-190.

Ranganathan, S. M. (2000). Photoresist-Derived Carbon for Microelectromechanical Systems and Electrochemical Applicaitons. *Journal of the Electrochemical Society* , 277-282.

Rochelle M. Cornell., U. S. (2003). *The iron oxides: structure, properties, reactions, occurrence and uses.* VCH Verlagsgesellschaft mbH.

Schreier, P. G. (2005). *MEMS based biosensor brings the hope of disposable DNA detector.* Retrieved from Comsol News No.1.

Shipley. (1998). MSDS for S-1813 Photoresist.

T.P. Misko, M. R. (1987). Nerve growth factor in neuronal development and maintenance. *J. Exp. Biol* , 177-190.

Xian Huang, S. L. (2009). A MEMS affinity glucose sensor using a biocompatible glucose-responsive polymer. *Sensors and Actuators B: Chemical , 140* (2), 603-609.

Y. W. Fan, F. Z.-S. (2002). Culture of neural cells on silicon wafers with nano-scale surface topograph, Journal of Neuroscience Methods. *Journal of Neuroscience Methods , 120* (1), 17-23.

Zhang, N. K. (2002). Surface modification of superparamagnetic magnetite nanoparticles and their intracellular uptake. *Biomaterials , 23* (7), 1553–1561.

8 Appendix

8.1 Supplemental Thoughts on Experimentation

8.1.1 Pyrolysis Furnace

Controller for the furnace used for the pyrolysis, while tuned for a heating rate of 2°C, will not follow the heating slope exactly. The furnace will be activated when the set point temperature (the green numbers on the thermocouple controller labeled SP) is five degrees higher than the actual measured temperature (the large, red numbers on the thermocouple controller), and the activation will be noted by a small red dot appearing next to the "out" indicator on the bottom left corner of the thermocouple controller. It will then stop actively heating the tube when the measured (red number) temperature is five degrees above the set point (green number) temperature. However, the temperature will overshoot the set point by almost 40 degrees each time; the impulse of heat that the tube takes over the short period of time is enough to heat the entire tube well above the set point, and is well-insulated enough that the temperature does not drop any significant amount. While not an ideal temperature ramp, it is consistent with all previous experimentation done with the furnace.

8.1.2 Oxidation of the Magnetite of the carbon surface

During the pyrolysis procedure, the quartz chamber utilized to heat the substrates is flooded with nitrogen gas. The gas, compressed in a standard cylinder, is passed through a regulator and then controlled with a rotameter inside the hood, graduated every five standard cubic centimeters per minute (SCCM), ranging from zero to one hundred. The nitrogen is, as stated before, used to create an inert environment for the individual substrates to be heated in. The procedure calls for excess nitrogen, which has been established at 100 SCCM. If the flowrate is raised above 100 SCCM, one can hear the nitrogen escaping out of the outlet of the tube. This ensures that there is, indeed, only nitrogen in the vessel.

There were two runs where the flowrate of nitrogen to the quartz vessel was not maintained to be at or above 100 SCCM; one due to a leak in the regulator setup (resulting in the depletion of all nitrogen in the tank) and one run where the nitrogen flowrate was set to 30 SCCM after it had reached the 1000 C mark and the heating element was turned off for cooling. Both of these runs were carried out *ceteris paribus* with all other runs, including the location and order of the sleds. Both of these runs produced samples with a light red powder coating the surface. Upon wiping away the powder, either a dull matte finish was found on the carbon or it revealed the bare silicone wafer, neither of which were suitable for cellular evaluation. These are pictured below, in Figure 25.

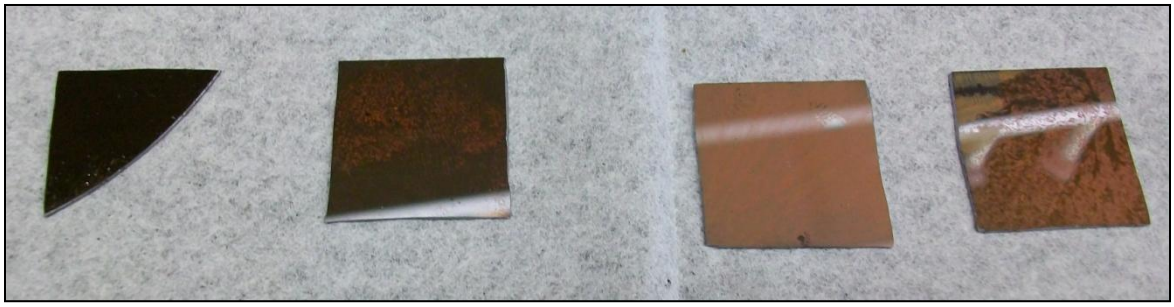

Figure 25: A selected representation of the samples during the low-nitrogen run. *From left to right:* Plain Carbon, FeO 0.2, FeO 0.5 and FeO 0.8.

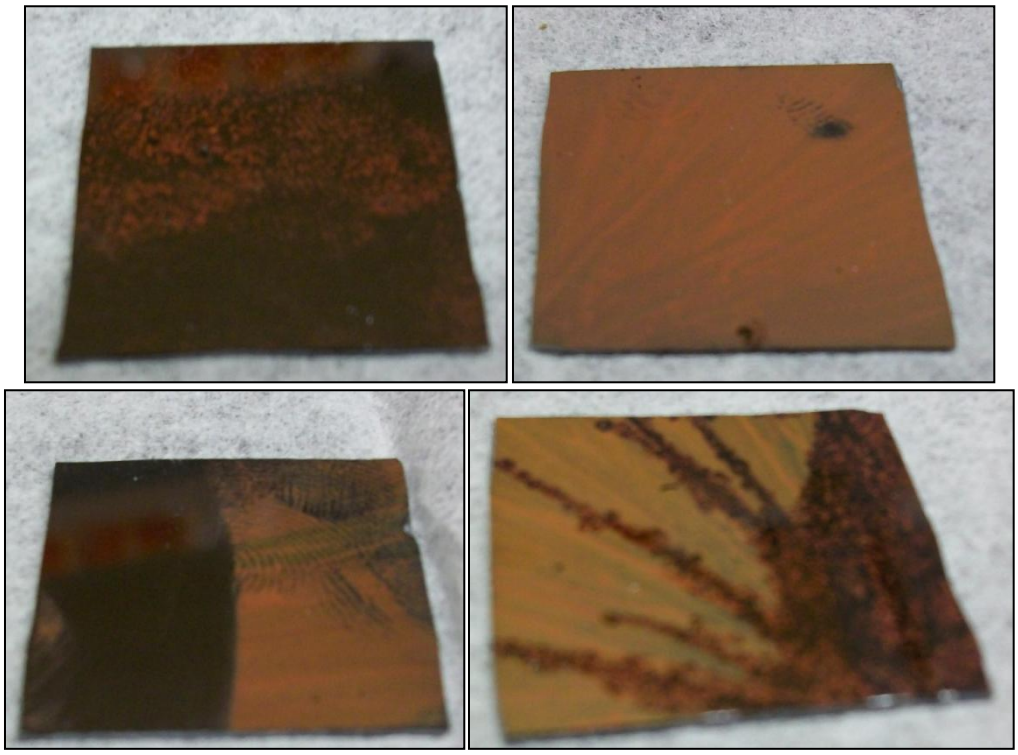

Figure 26: Pictures of substrates with greater detail. *Clockwise from top left:* FeO 0.2, FeO 0.5 shows a very thin layer over the whole surface, Fe 0.8 with a thin layer that follows the pattern from spin coating, and an FeO 0.5 sample with the powder wiped off of one side: notice the ease of release with the fingerprint markings on the right side.

While the characterization of the red-orange powder is not under the scope of this project's analysis, one would believe that it is the product of the oxidation of the Fe_3O_4 magnetite nanoparticles to the gamma phase of ferric oxide, γ-Fe_2O_3, also known as iron (III) oxide and more commonly red iron oxide[56]; the oxidation of magnetite to gamma-ferric oxide has been seen and documented in the field of metallurgy as early as 1968.[57] Gamma ferric oxide is commonly seen in a red-orange powder and is known to oxidize from magnetite (and other forms of Fe_3O_4) at high temperatures with the presence of oxygen. During normal pyrolysis procedures, the nitrogen flowrate is maintained, ruling out the

[56] (Cornell, 1996)
[57] (Gallagher, 1968)

possibility of a substantial amount of oxygen being present.[58] However, the reduced flowrate leads us to believe that oxygen was not kept out of the quartz vessel during the cool down of the quartz tube. When we look at the samples themselves, as seen in the pictures, no red powder is found on the plain carbon substrates, and there appears to be more red powder on the substrates with higher concentrations of magnetite nanoparticles, though a quantitative analysis was not performed.

It is believed that the lack of nitrogen decreased the pressure on the nitrogen side of the tube, as there was little to no flow of nitrogen to the vessel. There is, however, the outlet vent, which is under a hood ventilated at a rate of 181 fpm. Due to the decreased pressure on the nitrogen side, the air from the hood could flow into the vessel, introducing oxygen to the substrates. While the magnetite nanoparticles will modify the carbon surface during the pyrolysis, acting as a catalyst to change the surface morphology into complex carbon fibers, they could exist on the surface, especially as the mechanism of where and how the nanoparticles travel during the pyrolysis procedure is largely unknown, and therefore exist on the surface and interact with the oxygen. With the presence of oxygen (from the decreased pressure on the nitrogen side) and the elevated temperatures of the normal pyrolysis procedure, the red powder is believed to be γ-Fe_2O_3.

8.1.3 Imaging Procedure

The imaging process can be undertaken 24 hours after the substrates have been prepared for imaging. This time is required for the mounting media to set and be unobtrusive to the images. The microscope is a Nikon Eclipse E600, fitted with an RT Color SPOT camera, hooked up to a Windows 98 PC via dual serial port connections. The software used, SPOT, can be found on the desktop, and can be opened up first.

To ensure the longevity of the bulb for the microscope, one must check to see if it has seen on recently; it requires a 20 minute cool-down period. The black heat sink higher up (farthest away from the desk) on the backside of the microscope should be felt for heat. If it is still dissipating heat, wait until it is nearly room temperature; also, look for any notes around the keyboard or microscope controls that tell the last time it was used.

Once cool, two switches must be flipped; one on the SPOT power supply (for the camera) as well as the bulb power supply, labeled MERCURY-100W. These should be flipped and left on ten minutes prior to the taking of pictures. Again, this is for the longevity of the bulb used.

For our purposes, the microscope is used in a "clean" configuration; the darkening filters (found behind and to the left of the binoculars; black, rectangular plastic pieces labeled N4. N8 and N16) should be pulled out, as well as the filters on the right side of the microscope, located behind the positioning control stick. There are three chrome cylinders; they should not be pushed in. If they are, depressing the black lever directly above the engaged cylinder will release it. Once the microscope is ready, we can load a sample and begin the photography process. To load the sample, simply take the slide and place it in the slide holder.

[58] (Feitknecht, 1970)

The substrates, opaque, cannot be seen through normal microscopy, so we will use fluorescent light in order to capture the correct images. The DiI dye is florescent, and will show in the presence of green light. To filer this light, there is a slider directly below the binoculars on the front plate: it can slide between settings 1-4. The green light is setting three, with the other spectrums available.

Once the filter is selected for the correct light color, the cells can be viewed through any of the 10X, 20X, or 40X lens. After the lens is positioned, use the position control stick to travel longitudinally and latitudinal across the sample. Once the lens is over the substrate, we can open the shutter, the small circular control on the front panel. The shutter should be left closed at all times, unless tracing and finding a good area or taking the photograph. Once open, you will see the green light on the surface of the substrate. From here, ensure the horizontal pull bar next to the binoculars is pushed in, allowing all of the light to go to the binoculars. Lastly, one must focus the microscope on the cells. This can be done with the rough and fine knobs on the side of the microscope.

Once the cells to be imaged are aligned in the center of the sight, the shutter can be closed, the horizontal pull bar is pulled all the way out, to let light go to the camera and the shutter reopened. By striking F9 in SPOT, or going to Image -> Obtain Image, the picture will command the camera as determined in the exposure profile. The exposure profile can be tweaked and modified; this can be found through the menus. However, we have found that the ZZ-red and WPI templates were both adequate for capturing good data.